



Organic solvent-free fabrication of thin film polyamide/zeolitic imidazolate framework membranes for removal of dyes from water

Jose Miguel Luque-Alled ^{a,b,*}, Lidia Martínez-Izquierdo ^{a,b}, Patricia Gorgojo ^{a,b,c}, Carlos Téllez ^{a,b}, Joaquín Coronas ^{a,b,*}

^a Instituto de Nanociencia y Materiales de Aragón (INMA) CSIC-Universidad de Zaragoza, 50018 Zaragoza, Spain

^b Departamento de Ingeniería Química y Tecnologías del Medio Ambiente, Universidad de Zaragoza, 50009 Zaragoza, Spain

^c Department of Chemical Engineering, Faculty of Science and Engineering, The University of Manchester, Manchester M13 9PL, United Kingdom

ARTICLE INFO

Keywords:

Thin film nanocomposite membrane
Polyamide
Zeolitic imidazolate framework
Water nanofiltration
Dye removal

ABSTRACT

Thin film composite (TFC) polyamide (PA) membranes in combination with zeolitic imidazolate frameworks (ZIF), such as ZIF-8 and ZIF-93, have been fabricated using a novel approach based on vapor phase interfacial polymerization (VIP). These membranes have been investigated for nanofiltration (NF) of aqueous solutions of organic dyes, such as Rose Bengal (RB, 1017 Da), Sunset Yellow (SY, 452 Da) and Acridine Orange (AO, 265 Da). The preparation of the PA layer by VIP technique avoids the use of any organic solvent that is typically required in the conventional PA synthesis. Both ZIF-8 and ZIF-93 were initially synthesized using conventional procedures (methanol-based route) and incorporated to the PA layer in two different configurations: i) thin film nanocomposite with ZIF embedded within the PA film, and ii) bilayer membranes with a layer of ZIF between the support and the PA layer. The synthesis of ZIF-93 using a water-based route was developed for the bilayer configuration allowing for an organic solvent-free fabrication of PA/ZIF-93 bilayer VIP-TFC. These membranes showed the highest water permeances of 2.6, 3.4 and 2.2 L m⁻²h⁻¹ bar⁻¹ for RB, SY and AO, respectively. As compared to the control membrane VIP-TFC, this represents permeance increases of 69–117% and maintains high (greater than 99%) rejection of all the organic dyes. Membrane characterization demonstrated that the permeance enhancement for bilayer PA/ZIF-93 VIP-TFCs is related to an improved hydrophilicity, higher surface roughness and thinner selective layers. The prepared membranes demonstrated excellent cycle stability, maintaining their initial water permeance and dye rejection throughout 34 h of long-term operation, and being able to operate across the entire pH range studied (pH 3 to 9) without any detrimental effects on performance.

1. Introduction

Nanofiltration (NF) is a mature membrane technology that allows for an efficient removal of low molecular weight (MW) molecules and divalent salts from water and organic solvents [1]. Amongst many others, water NF has been successfully applied for removal of organic contaminants [2–4] and heavy metals in industrial water streams [5,6], for product isolation and processing in food technology [7], and for purification purposes in the pharmaceutical industry [8]. Due to significant ongoing research and constant improvements in the performance of NF membranes, NF is the highest growing technology amongst

all filtration-based water purification technologies [9]. Most commercial NF membranes are based on a thin film composite (TFC) membrane configuration, which typically consists of a 20–200 nm thick polyamide (PA) layer on top of a highly permeable porous polymer support, commonly polysulfone (PSF), polyethersulfone (PES), or polyimide (PI), that provides sufficient mechanical stability [10]. The ultrathin nature of the selective PA layer accounts for high water flux, whereas superior rejection properties arise from the typically highly crosslinked PA layer.

Membrane-based operations are often considered as a “clean” and “environmentally sustainable” technology due to their lower energy consumption as compared to the state-of-the-art technologies. However,

Abbreviations: NF, nanofiltration; TFC, thin film composite; TFN, thin film nanocomposite; PA, polyamide; RB, Rose Bengal; SY, Sunset Yellow; AO, Acridine Orange; VIP, vapor interfacial polymerization; TMC, trimesoyl chloride; MPD, phenylenediamine; 2-mim, 2-methylimidazole; 4-m-5-Imca, 4-methyl-5-imidazole-carboxaldehyde; HDA, hexanediamine.

* Corresponding authors at: Instituto de Nanociencia y Materiales de Aragón (INMA) CSIC-Universidad de Zaragoza, 50018 Zaragoza, Spain.

E-mail addresses: jose.luque@unizar.es (J.M. Luque-Alled), coronas@unizar.es (J. Coronas).

<https://doi.org/10.1016/j.cej.2023.144233>

Received 21 March 2023; Received in revised form 17 May 2023; Accepted 17 June 2023

Available online 20 June 2023

1385-8947/© 2023 The Author(s). Published by Elsevier B.V. This is an open access article under the CC BY-NC license (<http://creativecommons.org/licenses/by-nc/4.0/>).

membrane manufacturing processes raise many concerns from an environmental point of view due to the use of nasty organic solvents and generation of large amounts of chemical waste. During the fabrication of NF and reverse osmosis membranes, the PA layer is synthesized using a technique known as interfacial polymerization (IP) that involves a polycondensation reaction between a diamine monomer, typically *m*-phenylenediamine (MPD), in an aqueous solution and trimesoyl chloride (TMC) monomer dissolved in a water-immiscible organic solvent, commonly *n*-hexane or toluene. Attempts of getting rid of toxic solvents such as *n*-hexane or toluene by replacing them with other alternative solvents, e.g. isoparaffinic fluid [11], have shown a partial success. Although these procedures may result in high-performing membranes, after the reaction, unreacted TMC remains in the organic solution. In other words, after the reaction the solvent needs to be treated as a chemical waste before disposal due to the presence of TMC, significantly increasing the energy usage and the overall costs. Recently, our group reported the first preparation of TFC membranes by vapor IP (VIP), a strategy consisting of evaporating the TMC instead of dissolving it in a water-immiscible solvent [12]. In this method, TMC reaches the membrane support, where MPD molecules are impregnated within the pores, as a vapor phase and immediately reacts with MPD resulting in the formation of a PA layer. Therefore, this method emerges as an alternative to the conventional IP reaction and allows for low waste generation, improves the safety of workers by reducing their potential exposure to toxic substances, and mitigates costs associated with reagent and solvent recovery and disposal. In addition, this method is potentially scalable and economically affordable for the preparation of large industrial membranes. However, the performance of the vapor phase TFCs (VTFCs) still needs some improvement to equate that of conventional TFCs. In a previous work from our research group [12], VTFCs were investigated for aqueous NF of organic dyes and their performance was compared with TFCs prepared by the conventional IP technique. VTFCs showed excellent rejection (greater than 98%) of Rose Bengal (RB, 1017 Da), but rejection of smaller organic dyes Sunset Yellow (SY, 452 Da) and Acridine Orange (AO, 265 Da) was compromised (<98 % and < 94 %, respectively). On the contrary, conventional TFCs achieved exceptional rejection (greater than 98%) for all three dyes RB, SY and AO. Very recently, other authors [13,14] followed the same VIP technique to prepare NF membranes. Li et al. [13] prepared VTFCs membranes based on polycondensation reactions between β -cyclodextrins and TMC which achieved rejections above 90% for organic molecules larger than 400 Da. In another work, Karki et al. [14] reported the fabrication of PA membranes by VIP made of diethylenetriamine and TMC and containing TiO₂ nanoparticles (NPs) for heavy metal ions removal. Nevertheless, due to the early stage of the VIP technique, the performance of this sort of membranes can still be further improved by several means, including the choice of adequate monomers, optimization of the synthesis conditions (e.g. time, temperature, and control of humidity), and incorporation of nanomaterials or additives. As an alternative to membrane-based operations, there are some eco-friendly options available for removing contaminants, such as biochar derived adsorbents [15] and granular activated carbon from biomass waste [16].

Metal organic frameworks (MOFs) have received a lot of attention, due to their highly porous crystalline structures and controllable/narrow pore size distribution [17]. ZIF-8 is the most studied member of the zeolitic imidazolate framework (ZIF) family of MOFs due to its numerous advantages. ZIF-8 possesses large inner cavities with a diameter of 1.16 nm and a window opening with a diameter of 0.34 nm [18] which potentially allows the passage of water molecules and prevents transport for larger ones. In addition, ZIF-8 can be synthesized through several routes using mild conditions [19–21] and shows good stability in aqueous environments [22]. Methods have been proposed to incorporate ZIF-8 into PA membranes boosting the membrane performance. Zhao et al. [23] prepare PA/ZIF-8 membranes by two distinct approaches: i) dispersing ZIF-8 nanoparticles (NPs) in the acyl chloride/hexane solution and then blending ZIF-8 NPs with the PA layer, which is

known as thin film nanocomposite (TFN), and ii) preloading ZIF-8 NPs by vacuum filtration on top of the support followed by PA formation. The authors found that both types of membranes exhibited higher water permeances (up to 30% increase with the (ZIF-8)-preloaded membrane) and without compromising salt rejection as compared to TFCs. In a similar study, Wu et al. [24] explore the incorporation of ZIF-8 to PA membranes in two different configurations: i) ZIF-8 embedded within the PA layer (TFN), and ii) a layer of ZIF-8 grown on top of the PSF support prior to forming the PA layer (i.e. a bilayer configuration with the PA layer on top of the ZIF layer). Both strategies resulted in greater water permeances and higher rejections towards divalent salts and dyes as compared to solely PA membranes, which was attributed to higher surface roughness and more negatively charged membranes. Nonetheless, membranes in a bilayer configuration proved to be more efficient in increasing both water permeance and membrane rejection than TFNs. Wang et al. [25] also prepared bilayer PA/ZIF-8 membranes where the ZIF-8 layer was located between the PSF support and the PA layer. This intermediate layer of ZIF-8 was prepared using a novel technique based on a layer-by-layer fabrication method and the resulting membranes showed a 182% increase in water permeance without affecting the rejection properties.

Apart from ZIF-8, other ZIFs have also been proposed for their incorporation in NF membranes. ZIF-93 is particularly attractive since it shows a hydrophilic character due to the presence of an aldehyde group in the linker imidazole ring [26,27], on the contrary to ZIF-8 that is classified as a hydrophobic material. Paseta et al. [28] reported the implementation of PA/ZIF-93 membranes for the removal of pharmaceutical compounds from water. Due to the hydrophilic behavior and high porosity of the ZIF, the bilayer PA/ZIF-93 membrane led to a 144–256% increase in water permeance while maintaining rejection above 99%. In this same bilayer PA/MOF strategy, Berned-Samatan et al. [29], using a support of single-walled carbon nanotubes (SWCNTs), have recently studied the influence of ZIF-8 and ZIF-93 sublayers on the PA film, finding that the physicochemical properties of the ZIF and SWCNTs can influence the NF performance with notable improvements.

Here, we report, for the first time, PA membranes prepared by VIP together with MOFs (ZIF-8 and ZIF-93) for the removal of low MW organic molecules (RB, SY and AO dyes) from water. Amongst all the available MOFs, we chose ZIF-8 as it has been the most studied ZIF for NF applications and ZIF-93 due to its hydrophilic nature. As shown in the introduction section, the fabrication of PA/ZIF-8 and PA/ZIF-93 TFN membranes have been previously reported in the literature. However, the formation of bilayer membranes, specifically using ZIF-93, has received comparatively less attention in literature. In this work, the sublayer of ZIF-93 has been grown using a water-based route. Previously, ZIF-8 and ZIF-93 for membrane separations were only synthesized through the conventional organic solvent route. In addition, our approach focuses on the formation of the PA layer via a VIP approach that allows for an organic solvent-free synthesis of the PA layer. The VIP procedure has been improved, as compared to those previously reported, to achieve high rejection of organic dyes with a MW as low as 265 Da. So far, VIP-PA membranes reported in other studies were incapable of obtaining satisfactory rejection of molecules smaller than 400 Da [12,13]. In addition, demonstrating the flexibility of the VIP-PA approach, both bilayer and TFN membrane configurations were prepared through a more efficient procedure as compared to the conventional IP reaction involving organic solvents, since the absence of washing off during the PA synthesis does not propitiate the loss of MOFs. Due to the significantly distinct morphology of VTFCs as compared to conventional TFCs (i.e. remarkably different roughness and thickness of the PA layer), the influence on the PA layer due to the incorporation of MOFs to VTFCs remains unexplored so far. Prepared PA/ZIF membranes were characterized using scanning electron microscopy (SEM), atomic force microscopy (AFM), water contact angle (WCA), X-ray photoelectron spectroscopy (XPS) and transmission electron microscopy (TEM),

and the impact of the addition of ZIF-8 and ZIF-93 on the NF performance of the membrane was elucidated.

2. Material and methods

2.1. Materials

All materials were used as received. Deionized (DI) water with a conductivity of 1.3 $\mu\text{S}/\text{m}$ was used.

The following chemicals were involved in the synthesis of ZIFs. $\text{Zn}(\text{NO}_3)_2 \cdot 6\text{H}_2\text{O}$ (98%) was obtained from Scharlau. 4-methyl-5-imidazole-carboxaldehyde (4-m-5-Imca, 99%) was purchased from Fisher Scientific. 2-Methylimidazole (2-mIm, 99%), sodium formate (99%), ammonium hydroxide solution ($\text{NH}_4(\text{OH})$, 28.0–30.0% NH_3 basis) and 1-octanol (99%) were provided by Merck. Methanol (HPLC grade) was bought from Análisis Vínicos.

The following reagents and solvents were used for the synthesis of the polyimide P84® supports and the polyamide (PA) layer. Polypropylene nonwoven backing material was provided by Freudenberg Performance Materials, P84® powder –200 mesh- was purchased from HP polymer GmbH and Dimethyl sulfoxide (DMSO, 99.8%) was obtained from Carlo Erba reagents. Isopropanol (IPA, 99.9%) was purchased from Análisis Vínicos. Hexanediamine (HDA, 98%), MPD (99%) and TMC (98%) were bought from Merck. Polyethylene glycol (PEG, synthesis grade) was obtained from Scharlau Absolute ethanol (EtOH) was obtained from Gilca.

The following chemicals were employed for the filtration experiments. RB (95%), SY (90%), AO (55%), and PEG samples of different MWs (200, 400, 600, and 1500 Da) were purchased from Sigma Aldrich.

2.2. Synthesis of nanofillers ZIF-8 and ZIF-93

ZIF-8 was synthesized by a previously reported method [30]. Briefly, 1.467 g of $\text{Zn}(\text{NO}_3)_2 \cdot 6\text{H}_2\text{O}$ (4.93 mmol) and 3.245 g of 2-mIm (39.52 mmol) were dissolved in 150 mL of methanol, respectively. Once dissolved, the ligand solution (2-mIm) was added to the Zn^{2+} solution. The resultant solution was stirred for 30 min at room temperature giving rise to the MOF suspension. The MOF was then recovered by centrifugation at 9,000 rpm for 10 min and multiple washing steps with methanol. The final product was dried at 40 °C overnight.

ZIF-93 synthesis was carried out as reported by Pasetta et al. [31]. First, 0.882 g of $\text{Zn}(\text{NO}_3)_2 \cdot 6\text{H}_2\text{O}$ (2.96 mmol) and 2.610 g of 4-m-5-Imca (23.7 mmol) were dissolved in 60 mL of methanol each. Once the Zn^{2+} solution was added to the ligand solution the stirring continued for 20 min at room temperature giving rise to a cloudy suspension. ZIF-93 particles were recovered by centrifugation at 9,000 rpm for 10 min, washed with ethanol several times and dried overnight at room temperature.

2.3. Preparation of P84® supports

P84® porous supports were prepared via a non-solvent induced phase separation process following the procedure reported elsewhere [28]. A solution of P84® in DMSO at a concentration of 24 wt% was prepared with the aid of magnetic stirring. DMSO was chosen as a solvent as it is more environmentally friendly than other alternatives such as dimethylformamide and N-nethyl-2-pyrrolidone. This solution of P84® in DMSO was cast over a sheet of nonwoven polypropylene backing material attached to a glass plate. Using an automatic film applicator (Elcometer 4340) set at a gap of 250 μm and a speed of 0.04 $\text{m}\cdot\text{s}^{-1}$ the excess of casting solution was removed. Immediately, the nonwoven polypropylene containing the polymer casting solution was immersed in a coagulation bath containing DI water. After 10 min, the polymer has completely solidified, and the membrane supports were moved onto another water bath to remove any residue of DMSO inside of the support membrane pores and left for another 10 min. Then, the

supports were washed four times (1 h each) with IPA to remove any water from inside of the pores and immersed in a solution of HDA in IPA (120 $\text{g}\cdot\text{L}^{-1}$) for 16 h resulting in crosslinked P84® membrane supports of thicknesses of $\sim 150\text{--}200\text{ }\mu\text{m}$. Finally, the supports were washed twice with IPA for 1 h and immersed in a solution containing PEG/IPA (3:2, v/v) for preservation.

2.4. Preparation of VTFC and VTFN membranes

TFC and TFN membranes were fabricated on top of the prepared P84® supports by a vapor phase interfacial polymerization technique (exemplified in Fig. 1), denoted as VTFC and VTFN membranes, respectively.

For the preparation of VTFC membranes, P84® support discs of 19.6 cm^2 were impregnated with an aqueous solution of 2% (w/v) of MPD for 2 min. Then the excess solution was removed using a rubber brayer roller and immediately transferred inside of a vacuum oven at 60 °C and 40 mbar for 15 min to remove water molecules from the pores of the support. The IP reaction took place in a Teflon-lined stainless-steel autoclave. 10 mg of TMC was placed at the bottom of the Teflon liner closed using the P84® support as a lid (with the side of the support that contains the MPD facing down and exposed to TMC vapors). The Teflon liner was sealed by means of the stainless-steel body to prevent any TMC from being released and any air coming in. The autoclave was then placed in a preheated oven at 70 °C for 30 min. Afterwards, the autoclave was cooled down with water, the membrane was taken out and immersed in a Petri dish with DI water for 10 min, and finally transferred to a new Petri dish with fresh water and stored at 4 °C until further use.

VTFN membranes of ZIF-8 and ZIF-93 were fabricated following the same procedure (Fig. 1), but the solution of 2% of MPD in water (w/v) also contained the ZIF dispersed at a concentration of 0.2% (w/v).

All membranes were used in a period of maximum 5 days from preparation. Fabrication details of all membranes can be found in Table 1.

2.5. Preparation of polyamide/ZIF bilayer VTFC membranes

The fabrication of PA/ZIF membranes was carried out using a two-step approach (exemplified in Fig. 1): 1st step) ZIFs were deposited on top of the P84® support, and 2nd step) the PA layer was prepared on the ZIF/P84® membrane following the procedure described above for VTFC membranes. Deposition of ZIFs was done by direct crystallization on the surface of P84® as follows.

ZIF-8 and ZIF-93 layers were crystallized on P84® supports using a similar procedure to that described elsewhere [28] which involves the use of organic solvents, and then denoted as organic solvent route (OSR). Two solutions were prepared under stirring for at least 2 h: i) an aqueous solution of $\text{Zn}(\text{NO}_3)_2 \cdot 6\text{H}_2\text{O}$ at a concentration of 0.15 $\text{mol}\cdot\text{L}^{-1}$, and ii) a solution of the ligand (2-mIm for ZIF-8 and 4-m-5-Imca for ZIF-93) at a concentration of 0.25 $\text{mol}\cdot\text{L}^{-1}$ along with sodium formate at a concentration of 0.25 $\text{mol}\cdot\text{L}^{-1}$ in a mixture of methanol/1-octanol (2:1, v/v). 10 mL of the aqueous solution was poured over the P84® support and left for 1 h to allow effective impregnation of its pores. The excess solution was subsequently decanted, and remaining drops were eliminated using a rubber brayer roller. The ligand solution was then added and after 1 or 30 min for ZIF-8 and 1 min for ZIF-93, ethanol in excess was poured to stop the reaction and the membranes were washed with ethanol and water. Afterwards, the membranes were immersed in ethanol for 10 min and left to dry inside of a fume hood for 30 min prior to the preparation of the PA layer.

ZIF-93 was also crystallized on top of P84® using a synthetic route previously described that reports the synthesis of ZIF-93 in powder using water as the only solvent [32], the so-called water-based route (WBR). However, the procedure was adapted for the preparation of PA/ZIF bilayers. In this case, the reaction was done in two steps to ensure the

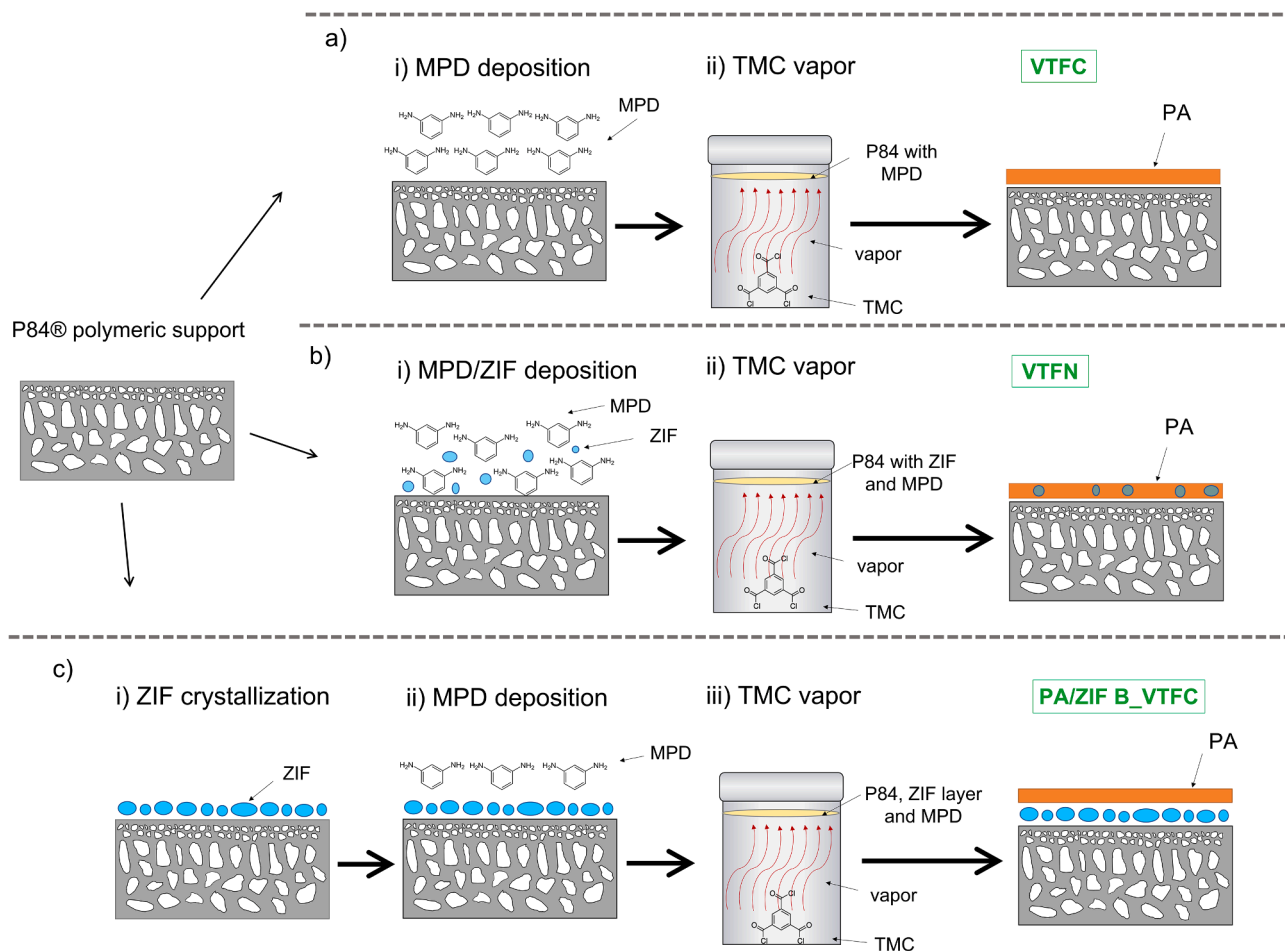


Fig. 1. Fabrication of VTFC (a), VTFN membranes (b), and Polyamide/ZIF bilayer VTFC membranes (c).

Table 1

Fabrication details of all membranes prepared including membrane code, type of ZIF and synthetic route used, membrane configuration, and type of IP reaction.

Membrane code	ZIF NPs (route of synthesis)	Membrane configuration	IP reaction
TFC	–	TFC	Conventional
VTFC	–	TFC	Vapor
VTFN-Z8	ZIF-8 (Organic solvent route)	TFN	Vapor
B_V-Z8	ZIF-8 (Organic solvent route)	Bilayer	Vapor
VTFN-Z93	ZIF-93 (Organic solvent route)	TFN	Vapor
B_V-Z93	ZIF-93 (Organic solvent route)	Bilayer	Vapor
W-B_V-Z93	ZIF-93 (Water-based route)	Bilayer	Vapor

correct deposition of ZIF-93 on top of the P84® support. First, an aqueous solution of $\text{Zn}(\text{NO}_3)_2 \cdot 6\text{H}_2\text{O}$ and 4-m-5-Imca at concentrations of $0.063 \text{ mol}\cdot\text{L}^{-1}$ and $0.14 \text{ mol}\cdot\text{L}^{-1}$, respectively, was added over the P84® support and left for 1 h to impregnate its pores. Then, the excess solution was pushed out using a rubber brayer roller and a solution of $\text{NH}_4(\text{OH})$ in water at a concentration of 1.2% (v/v) was added triggering ZIF-93 crystallization. After 1 min of reaction, DI water was supplied to dilute the base solution and to stop the reaction, then the membrane was

washed with water three times and left to dry at room temperature prior to the IP synthesis (following the same procedure described in previous section 2.4 for VTFC membranes).

All bilayer membranes prepared can be found in Table 1 along with their fabrication details and membrane codes.

2.6. Characterization

ZIFs were characterized using X-ray diffraction (XRD), thermogravimetric analysis (TGA), transmission electron microscopy (TEM) and N_2 sorption and desorption experiments. Thermogravimetric analysis (TGA) was carried out using a Mettler Toledo TGA/STDA 851e. Small amounts ($\sim 3 \text{ mg}$) of ZIF powder were placed in $70 \mu\text{L}$ alumina pans and heated under an airflow ($40 \text{ cm}^3 (\text{STP}) \text{ min}^{-1}$) from 35 to 700°C at a heating rate of $10^\circ\text{C min}^{-1}$. Crystallinity of ZIF was analyzed by X-ray diffraction using a reflection-transmission spinner stage with a zero-background sample holder on a PANalytical Empyrean-Multipurpose (Malvern Panalytical Ltd) equipment with a $\text{Cu K}\alpha$ ($\lambda = 1.542 \text{ \AA}$) rotating anode operating at 40 kV and 80 mA. TEM images were obtained using a Tecnai T20 microscope (ThermoFisher company) at an accelerating voltage of 300 kV and holey Carbon support films on Copper 300 square mesh (Aname). N_2 adsorption–desorption isotherms were obtained using a Micromeritics Tristar 3000 equipment at -195.8°C and the Brunauer-Emmett-Teller (BET) surface area was generated by the Micromeritics software analysis. The samples were degassed for 8 h under vacuum at 200°C (with a heating rate of $10^\circ\text{C min}^{-1}$) prior to the sorption measurements.

VTFCs, VTFNs and PA/ZIF bilayer VTFCs membranes were characterized by SEM, AFM, XPS, TEM, and water contact angle (WCA)

measurements. SEM images were acquired using a FEI-Inspect F20 microscope operating at 30 kV and equipped with an energy-dispersive X-ray detector. AFM characterization was carried out at ambient pressure by a Bruker MultiMode 5 scanning probe microscope using a tapping mode, a scan rate of 1 Hz and an amplitude of roughly 250 mV. XPS measurements were acquired using a Kratos Axis Ultra spectrometer with a monochromatic Al K α (1486.6 eV) X-ray source operating at 10 mA, 15 kV and a power of 150 W, and analyzed using CASAXPS software. The full-width-at-half-maximum (FWHM) at optimum conditions for an Ag 3d 5/2 high-resolution spectrum is 0.48 eV. WCA measurements were obtained using a Krüss Drop Shape Analyzer 10 MK2 at 25 °C and the reported values are the average of three measurements of each membrane. Ultrathin (~70 nm) TEM specimens were obtained by ultramicrotomy of the membranes embedded in epoxy resin at room temperature using a Leica EM UC7 ultramicrotome device and a diamond knife. Membranes were embedded in EMBed 812 epoxy resin overnight under vacuum and then, the resin was left to polymerize at 60 °C for 48 h. The block of resin was first trimmed using a glass knife and finally cut with a diamond knife. The diamond knife was positioned at 6°, and the step size and speed were set at 70 nm and 1 mm/s, respectively. Ultrathin TEM specimens were dropped into DI water and transferred to carbon 300 mesh copper grids. TEM imaging was performed using the same equipment and conditions mentioned above. Molecular weight cut-off (MWCO) experiments were carried out using PEG solutions of different MWs (200, 400, 600, and 1500 Da) in water at a concentration of 5 g·L⁻¹. The retentate and permeate solutions were analyzed using a total organic matter (TOC) TOC-L Series analyzer from Shimadzu.

2.7. Water nanofiltration experiments

The membranes were subjected to activation through filtration with DMSO prior to the filtration experiment. This post-treatment has been proven to effectively enhance membrane flux while preserving rejection properties, which can be attributed to the removal of unreacted monomers and polymer chain swelling [33]. Filtration experiments were performed using a Sterlitech HP4750 dead-end membrane module and aqueous solutions of dyes at a concentration of 20 mg·L⁻¹. Three dyes of different MW were chosen: i) RB (MW = 1017 Da), SY (MW = 452 Da) and AO (MW = 265 Da). These three dyes were chosen in order to cover a wide range of MW (from 265 to 1017 Da) and to study the rejection towards electrically charged dyes (negatively charged RB and SY, and positively charged AO). Experiments were performed at 20 bar of transmembrane pressure and 20 °C using an effective membrane area of 4.9 cm² and 250 mL of feed volume. The following equations were used to calculate the flux (L m⁻²h⁻¹), permeance (L m⁻²h⁻¹ bar⁻¹) and rejection (%):

$$Flux = \frac{V}{A \cdot t} \quad (1)$$

$$Permeance = \frac{Flux}{\Delta P} \quad (2)$$

$$Rejection(\%) = \left(1 - \frac{C_{permeate}}{C_{retentate}}\right) \cdot 100 \quad (3)$$

where V accounts for the volume (L), A for the membrane area (m²), t for the permeation time (h), and ΔP for the transmembrane pressure (bar). $C_{permeate}$ and $C_{retentate}$ represent the concentrations of dyes (mg·L⁻¹) in the permeate and retentate side, respectively, and were obtained using a UV-Vis Jasco V-670 spectrophotometer and water as a solvent. Absorbance values were related with the concentration of dyes in water by an equation obtained from calibration curves for each dye.

3. Results

The advantages of the vapor phase interfacial polymerization, already quoted for VTFC membranes, relate to the saving of reactants and the elimination of the use of organic solvent (typically n-hexane with the TMC monomer) for the synthesis of the polyamide [12]. In the current work this methodology has been extended to membranes containing MOFs (see Fig. 1). As compared to our previous report in which VTFC membranes were also fabricated [12], the method proposed in this report for the bare synthesis (without MOF) of VTFC membranes involves higher reaction temperatures (from 40 to 70 °C) which allows for shorter vapor interfacial polymerization times (30 min instead of up to 60 min). However, this did not alter the mechanism of membrane formation in which TMC is deposited from the vapor phase on the support surface impregnated with the MPD monomer without the needing of any organic solvent. As it will be shown below, the use of higher temperature during VIP allows for obtaining similar separation properties for TFC and VTFC membranes. Besides, the incorporation of suitable MOFs, either as NPs or as a continuous layer to obtain the so-called PA/MOF bilayer membranes, further enhances the membrane performance as compared to both TFCs and bare VTFCs.

3.1. Characterization of ZIF-8 and ZIF-93

The crystalline structure and purity of both MOFs were revealed from the XRD patterns of ZIF-8 and ZIF-93, which are shown in Fig. S1. Peak positioning of synthesized nanomaterials match those of the simulated ZIFs (sod and rho type structures for ZIF-8 and ZIF-93, respectively), supporting their effective synthesis [34,35]. TGA analyses under air atmosphere were used to study their thermal stability and the corresponding thermograms are shown in Fig. S2. The maximum degradation of ZIF-8 occurs at 450 °C whereas the one of ZIF-93 happens at 400 °C, evidencing that ZIF-8 has a higher thermal stability than ZIF-93. The residues at 700 °C can be attributed to inorganic ZnO [36]. From these thermograms, not showing significant weight losses at low temperature, it can also be confirmed that ZIFs have been correctly activated and that the unreacted linker molecules inside their pores can be considered negligible for the current purpose [31]. In line with this activation, the specific surface areas of the ZIFs calculated from the N₂ adsorption isotherms by the BET method of 1350 and 783 m² g⁻¹ for ZIF-8 and ZIF-93, respectively, are high and in accordance with the values reported in the literature [21,31]. N₂ adsorption/desorption curves, depicted in Fig. S3, correspond to the pseudo-type I IUPAC classification of adsorption/desorption isotherms where a hysteresis loop is observed between 0.9 a 1 P/P₀. This behavior is typical of microporous materials [37] with steep adsorption in values close to P/P₀ = 1 related to capillary condensation between nanoparticle spaces. TEM images reveal particle sizes of around 20 and 50 nm for ZIF-8 and ZIF-93, respectively (Fig. S4), compatible with either the preparation of nanoparticles very suitable for VTFC membranes or the crystallization of thin MOF layers enough to enhance the membrane separation properties without adding too much mass transfer resistance.

3.2. Membrane characterization

Top-view SEM images were used to investigate ZIF crystallization on P84® supports. Fig. 2a reveals that ZIF-8 was successfully synthesized after 30 min of reaction, whereas after 1 min of reaction only few NPs could be found (Fig. S5). However, for the synthesis of ZIF-93, a large number of NPs were already synthesized after 1 min as shown in Fig. 2b. The methods used to synthesize ZIF-8 and ZIF-93 are identical, except for the fact that a different ligand was employed, which evidence that the crystallization of ZIF-93 is much faster than that of ZIF-8. Indeed, ZIF-8 had previously been synthesized over PES supports using a very similar method and the authors reported that a minimum time of 15 min was required to perceive the presence ZIF-8 [38]. Fig. 2c unveils that

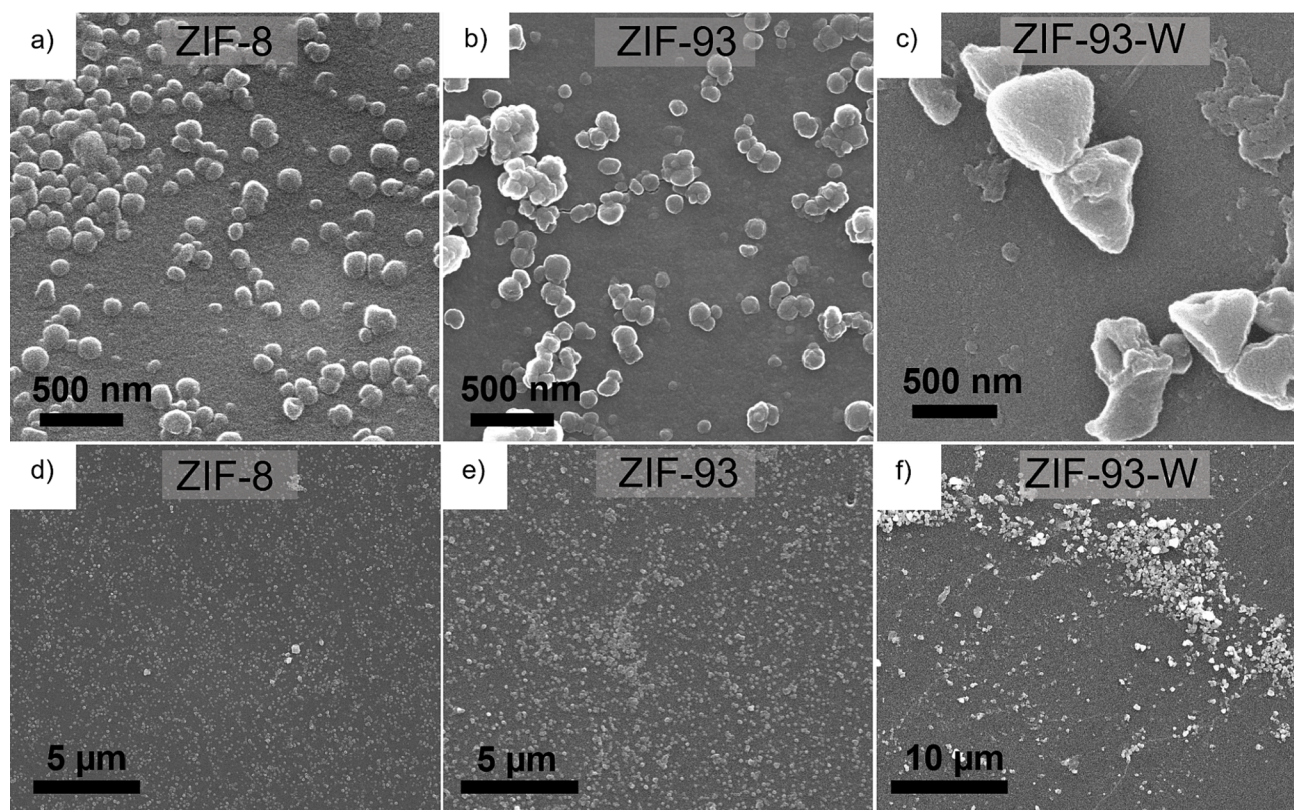


Fig. 2. Top-view SEM images of ZIF-8 (a and d), ZIF-93 (b and e), and water-based ZIF-93 (c and f) crystallized on top of the P84® supports. Fig. 2d-f corresponds to lower magnification of images of Fig. 2a-c.

ZIF-93 NPs prepared by WBR are significantly bigger and have more irregular shapes as compared to those synthesized by OSR (Fig. 2b). Fig. S5b, corresponding to ZIF-93-W (crystallized by WBR), shows the presence of NPs with very different lateral sizes ranging from 40 to 500 nm, approximately. Fig. 2d-f correspond to lower magnification SEM images of ZIF-8 (30 min of reaction, OSR), ZIF-93 (1 min of reaction, OSR), and ZIF-93-W (1 min of reaction, WBR), respectively. ZIF-8 and ZIF-93 synthesized by OSR produce a higher coverage of the P84® support as compared to ZIF-93 synthesized using WBR, ZIF-93-W. Fig. S6 shows the EDX spectra of ZIF-8, ZIF-93 and ZIF-93-W, which reveal a significant amount of Zn in all cases, providing further evidence of ZIF formation.

To gain further insights into the properties of ZIF-93 NPs synthesized via OSR and WBR, a bulk synthesis of these materials was performed for a comprehensive structural characterization. The obtained XRD (Fig. S7a) patterns confirm that the synthesized powders exhibit a crystallographic structure that is consistent with that of ZIF-93. Similar TGA curves were also obtained for both ZIF-93 synthesized via OSR and WBR (Fig. S7b). TEM analysis (Fig. S8) reveals that ZIF-93 synthesized through the WBR exhibits larger and more irregular shapes compared to those prepared using OSR. This observation is consistent with the findings discussed above regarding SEM characterization of ZIF-93 synthesized on P84® supports via OSR and WBR.

Top-view SEM images of selected membranes were acquired to study the morphology of the synthesized PA layer. Fig. 3a, corresponding to VTFC membranes, shows a fairly smooth surface where few irregularities are observed, similar to the morphology observed in our previous publication [12]. However, this morphology is very different from the characteristic rough surfaces of conventional PA TFCs where ridge and valley structures having earlike wrinkles are prevalent (Fig. S9a). Fig. 3b corresponds to PA/ZIF-93 bilayer VTFC membranes (B.V-Z93) and shows the presence of wrinkles and polymer veins resembling the characteristic structure of conventional PA TFCs.

Fig. 3c-d displays the two most predominant features observed in PA/ZIF-93 (by WBR) bilayer VTFC membranes (W-B.V-Z93): i) ridge and valley morphology and earlike wrinkles (Fig. 3c) and ii) abundant presence of nodes (Fig. 3d). It has been hypothesized that ZIF imidazole groups can establish π - π interactions with MPD monomers promoting the accumulation of monomers and the formation of more crumpled surfaces [23]. On top of that, ZIF-93 has a hydrophilic character due to the presence of an aldehyde group within the structure of the 4-m-5-Imca ligand. This may result in higher wetting of the ZIF-93 surface by the MPD aqueous solution as compared to bare P84® supports, as well as H-bonding interactions may occur between aldehyde groups and MPD molecules. The strong adsorption properties of ZIF NPs are also expected to play a significant role; in fact, even if ZIF-93 pore aperture is 0.36 nm [39], this MOF can experience the so-called gate opening allowing the inclusion of large molecular species in its much larger cavities of 1.8 nm [40]. The membranes undergo a heat treatment at 60 °C for 15 min prior to supplying TMC, where most of water molecules are expected to be removed, but the intrinsic porosity of ZIFs can aid in retaining water and MPD molecules. In all above cases, the result is a MPD-richer area and the subsequent formation of more prominent features, such as earlike wrinkles, leading to a ridge and valley morphology [23–25,41]. In addition, Fig. 3d shows numerous bumps in a nodular shape which are believed to arise from PA chains coating the ZIF-93 particles [24,25]. These round-shaped bumps have diameters between 100 and 600 nm, which is fairly similar to the size of ZIF-93 NPs shown in Fig. 2c. Fig. S10 displays the EDX spectrum of one of the nodes, where peaks corresponding to Zn are observed, in agreement with the existence of ZIF-93 NPs underneath. When comparing the morphology of both PA/ZIF-93 bilayer membranes, i.e. B.V-Z93 (ZIF-93 by OSR) in Fig. 3b and W-B.V-Z93 (ZIF-93 by WBR) in Fig. 3c-d, it seems that more protuberances are observed for the latter. This suggests that the bigger particle size and more irregular shape of ZIF-93 NPs synthesized by WBR (as seen in Fig. 2) is beneficial for the generation of rougher membrane

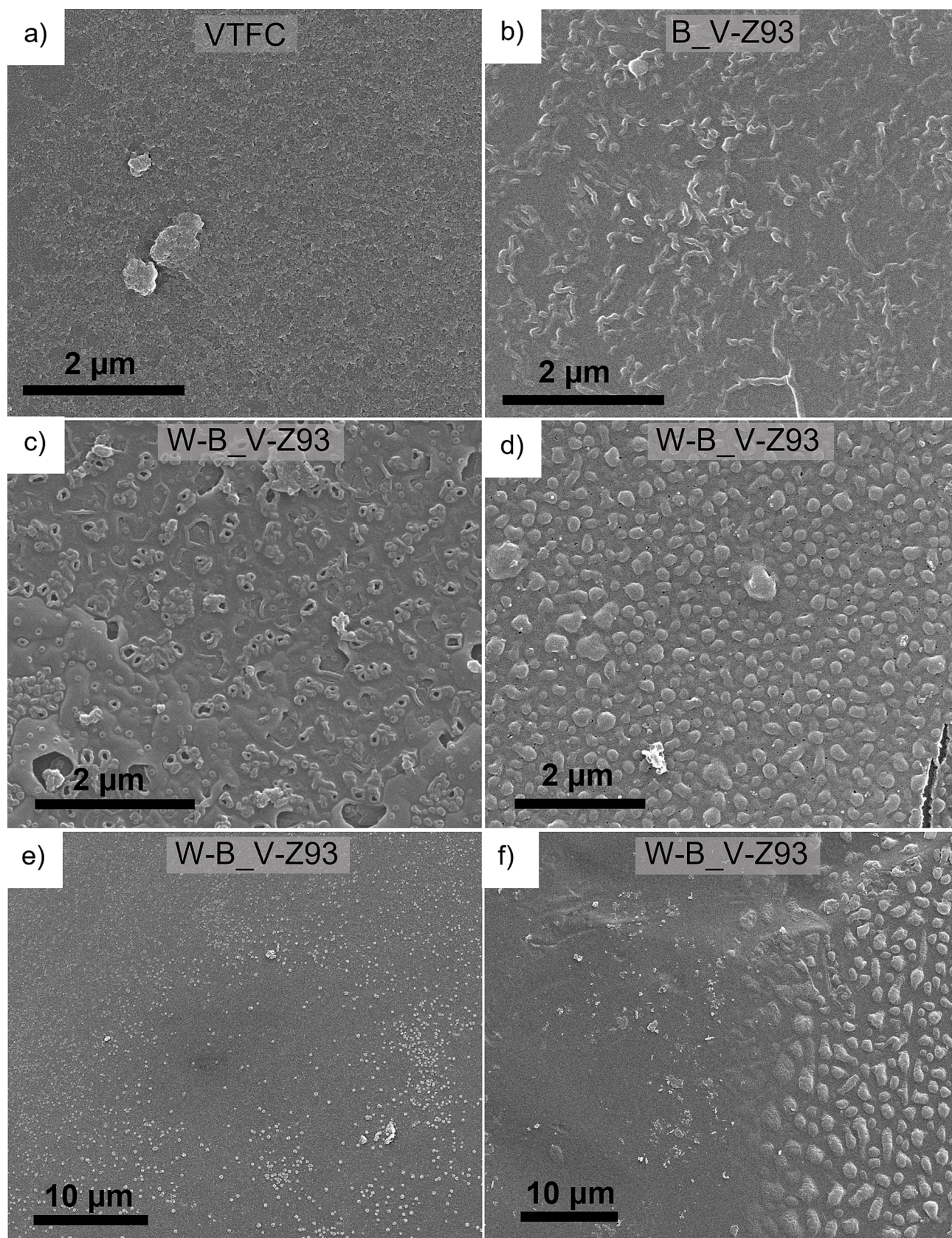


Fig. 3. Top-view SEM images of VTFC (a), B_V-Z93 (b) and W-B_V-Z93 (c-f) membranes.

surfaces. SEM images in Fig. 3e-f correspond to W-B-Z93 at lower magnification and show that these features, although they predominate along the surface of the membrane, are found together with smoother areas similar to those seen in VTFCs due to non-uniform coverage of the support with the NPs as observed in Fig. 2f.

A top-view image of PA/ZIF-8 bilayer VTFC membrane (B_V-Z8) is presented in the supporting information (Fig. S9b) and also exhibits wrinkles and polymer veins, although they are less prominent and abundant than those observed in B_V-Z93, possibly due to the higher hydrophobicity of ZIF-8 as compared to ZIF-93. SEM images of VTFC-Z8 and VTFC-Z93 are included in the supporting information, Fig. S9c and Fig. S9d, respectively. VTFC-Z8 shows a smooth surface with abundant craters. VTFC-Z93 shows a smooth surface similar to that of VTFC (see Fig. 3a). Differences between the two types of VTFC membranes may be due to agglomeration of the NPs; the hydrophilic ZIF-93 is expected to give rise to more stable dispersions in water, and then suffer less agglomeration as compared to hydrophobic ZIF-8. A better dispersion of the NPs in the polymer matrix is expected to have a lower influence on the morphology of the PA layer.

AFM images in Fig. 4a-d confirm the existence of large differences in the surface roughness of VTFC and W-B_V-Z93 membranes. AFM images agree with what was suggested by SEM analysis, i.e. VTFC shows a smooth surface whereas W-B_V-Z93 exhibits a rough surface containing abundant nodular protuberances. Fig. 4e shows that the presence of a ZIF-93 layer leads to a 4.5-fold increase in the roughness parameters Ra and RMS. Previous studies report that the formation of bilayer membranes increased membrane roughness [23,24,28]. Interestingly, Wu et al. [24] prepared bilayer PA/ZIF-8 membranes and found that the highest surface roughness did not relate to the highest support coverage with ZIF-8, which supports the findings in this manuscript, suggesting that a partial coverage of the support can still result in a substantial increase in surface roughness. SEM images encounter a much smoother surface for VTFC membranes in comparison with conventional TFCs. This is confirmed by roughness measurements obtained by AFM since the Ra and RMS values found for VTFC (3 and 5, respectively) are much lower than those seen for TFC membranes prepared using MPD and TMC monomers and P84® as a support (Ra of 12 nm and RMS of 15 nm) [28]. AFM images of VTFC-Z93 and VTFC-Z8 can be found in the supporting information (Fig. S11). Similar to that observed by SEM (Fig. S9), VTFC-Z93 exhibits a relatively flat surface with small irregularities, while VTFC-Z8 shows numerous craters. The roughness parameters, Ra and RMS, for both VTFC-Z93 (13 and 16 nm, respectively) and VTFC-Z8 (15 and 19 nm, respectively), are considerably higher compared to those of the VTFC membrane (3 and 5 nm, respectively). This increase in surface roughness is consistent with the presence of ZIF NPs within the thin PA layer.

Tuning the hydrophobicity/hydrophilicity of the PA layer by adding MOF has been widely reported [25,28]. Fig. 4e shows WCA values of all membranes prepared by the VIP technique. A WCA value of 71.2° was obtained for VTFC membranes, which corresponds to the characteristic value of a PA layer prepared using MPD and TMC monomers over P84® [28,42]. The incorporation of hydrophobic ZIF-8 as both TFN (VTFC-Z8) and bilayer membrane (B_V-Z8) increased the membrane WCA (75.5° and 76.0°, respectively) as compared to that of VTFC, whereas when using hydrophilic ZIF-93 (VTFC-Z93, B_V-Z93 and W-B_V-Z93) lower WCA values (61.0°, 64.4° and 63.9°, respectively) were observed. Values for VTFC-Z8 and B_V-Z8 are similar to those found by other authors when using ZIF-8 in TFNs [42] or as a bilayer membrane [25]. When hydrophilic ZIF-93 NPs are incorporated, the formation of TFNs (VTFC-Z93) results in more hydrophilic membranes as compared to both bilayer membranes (B_V-Z93 and W-B_V-Z8), in agreement with Paseta et al. [28]. Besides, the crystallization route of the ZIF-93 sublayer (OSR and WBR) in the bilayer configuration (B_V-Z93 or W-B_V-Z93, respectively) seems not to affect the WCA of the membranes since the chemical structure of ZIF-93 remains the same.

Fig. 5a-d shows cross-sectional TEM images of VTFC (a and c) and W-

B_V-Z93 (b and d) membranes. The synthesized PA layer in VTFC is noticeable thicker as compared to that in W-B_V-Z93. Although TEM images only show a tiny portion of the membrane, this thickness difference has been also observed in TEM specimens corresponding to other membrane sections (Fig. S12, S13) which suggests that this tendency could be predominant throughout the whole membrane surface. The existence of a thinner PA layer in W-B_V-Z93 can be explained by the higher membrane roughness and surface area, i.e., MPD molecules tend to concentrate around hydrophilic ZIF-93 creating crumpled figures as those seen in the SEM images (Fig. 3c-f), whereas in VTFC MPD molecules are more homogeneously distributed along the support surface producing a thicker PA layer. In Fig. 5b and Fig. S12 (TEM images), as well as in Fig. 3d (SEM images), all corresponding to W-B_V-Z93, the presence of several nodes can be identified. All these nodes have spherical or ovoidal shapes with diameters ranging from 60 to 400 nm, and all are covered with a well-defined PA layer. The origin of the nodes seems to be related to the presence of ZIF-93 NPs. As previously discussed, ZIF-93 NPs can promote the formation of protuberances on the PA layer due to interaction with water molecules and MPD monomers. Another hypothesis is that the nodes may also hold ZIF-93 NPs underneath. The size of the nodes observed by TEM (Fig. S13) are similar to the size of ZIF-93-W in the SEM images (Fig. S5) and of the nodes found on the surface of W-B_V-Z93 by SEM (Fig. 3d). EDX/SEM analysis of one of these nodes (Fig. S10) encounters the presence of significant Zn suggesting the existence of ZIF-93 NPs below the PA layer.

XPS analysis was carried out to investigate the chemistry of VTFC and W-B_V-Z93 membranes. High resolution spectra of C 1s, O 1s, N 1s and Zn 2p are found in Fig. S14-S17. The presence of small quantities of Zn was found in W-B_V-Z93 membranes, probably due to the existence of a ZIF-93 layer below the PA layer. However, the XPS probe has an estimated penetration depth of around 3–10 nm, which is shorter than the thickness of the PA layer observed by TEM (~15–20 nm). Then, the presence of Zn²⁺ can be explained by different reasons: i) existence of thinner PA layers at certain regions, ii) leftover Zn²⁺ that did not crystallize but remained in the membrane due to electrostatic interactions with functional groups in P84® or/and MPD molecules, and iii) leakage of Zn²⁺ atoms from ZIF-93 due to the generation of HCl during the polymerization reaction to form the PA layer [43]. Table S1 shows the atomic % (at. %) of both membranes, which was calculated from the spectrum areas. Comparison between C/N and O/N atomic ratios is often used to evaluate the degree of crosslinking of the PA layer [12,44]. Due to the presence of ZIF-93 NPs, the at. % compositions corresponding to the PA layer in W-B_V-Z93 membranes need some correction. Thus, the contribution of ZIF-93 to the at. % was calculated (from the empirical formula C₁₀H₁₂N₄O₂Zn) and deducted from the experimentally obtained values in Table S1. C/N and C/O ratios for the PA layer in W-B_V-Z93 were calculated and, if possible, correlated with the crosslinking degree of the PA layer, i.e. lower C/N and C/O values are associated with a higher cross-linking degree. Membrane W-B_V-Z93 (after subtracting ZIF-93 contribution) shows a higher C/N ratio but a slightly lower C/O ratio as compared to VTFC; however, these differences are within the expected experimental error suggesting a similar degree of cross-linking for both membrane types. The incorporation of ZIF-93 is not expected to have a significant influence in the degree of reaction between MPD and TMC since, in the bilayer configuration, ZIF-93 NPs are located below the PA layer.

To assess the integrity of ZIF-93 during the VIP process and investigate potential changes to its structure or penetration of TMC into its cavities, an additional experiment exposing ZIF-93 to TMC vapors was conducted. This experiment was carried out under the same conditions used to prepare the VTFC membranes, i.e. 70 °C for 30 min in Teflon-lined stainless steel autoclave. Fig. S18 displays the XRD pattern and TGA analysis of ZIF-93 after treatment with TMC vapors. Based on the same XRD intensities at the same angle values and on the very similar TGA curves obtained, it can be concluded that no noticeable changes were produced in the atomic and chemical structure of ZIF-93 NPs. TEM

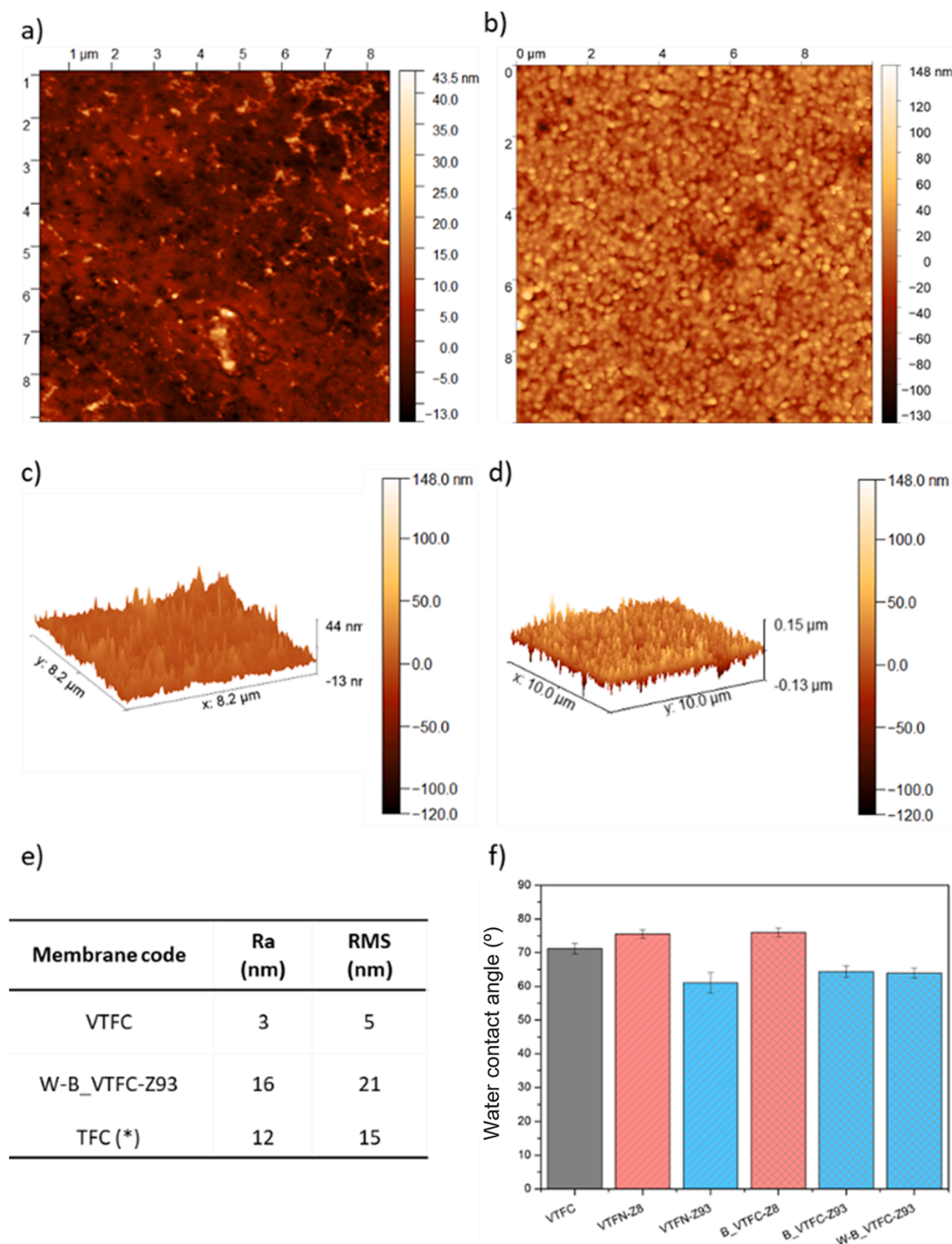


Fig. 4. 2D top-view AFM images of VTFC (a) and W-B_V-Z93 (b), 3D representations of VTFC (c) and W-B_V-Z93 (d) using the same color scale for both (from -120 to 248 nm), summary of Ra and RMS values (e), and WCA values of selected membranes (f). In Fig. 4e, asterisk (*) refers to TFC membranes reported by Paseta et al. [28]. Fig. 4f, red for ZIF-8 and blue for ZIF-93, while diagonal stripes account for VTFC membranes and crossing diagonal stripes for bilayer membranes. (For interpretation of the references to color in this figure legend, the reader is referred to the web version of this article.)

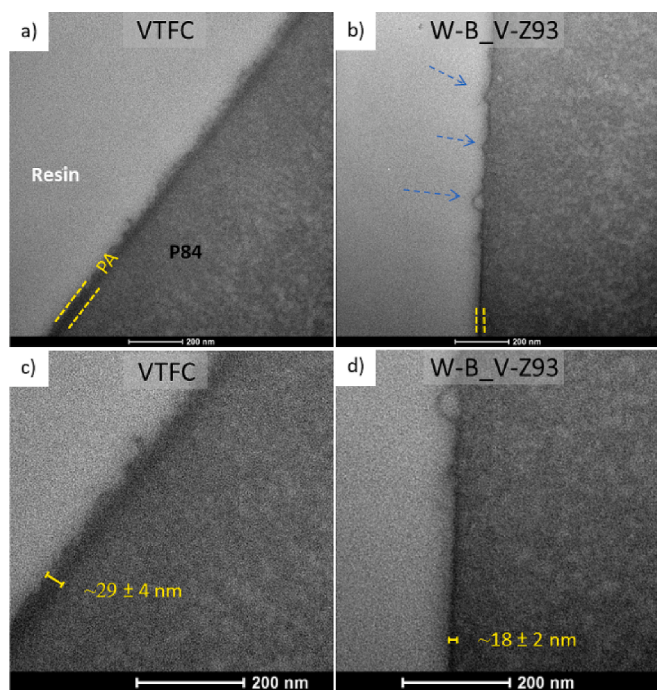


Fig. 5. Cross-sectional TEM images of VTFC (a and c) and W-B_V-Z93 (b and d). Fig. 5c and 5d correspond to amplified (x2) images of Fig. 5a and 5b, respectively. Blue arrows in Fig. 5b spot the presence of nodes. (For interpretation of the references to color in this figure legend, the reader is referred to the web version of this article.)

analysis (Fig. S19) reveals that the morphology of ZIF-93 NPs looks the same after the treatment with TMC vapor.

3.3. Membrane performance

The NF performance of TFC and VTFC membranes using solutions of RB and SY is compared in Fig. S20. TFC showed very similar water permeance for both RB and SY solutions, whereas, for VTFC membranes, the water permeance during the NF experiment with the SY solution was slightly higher than that with the RB solution. Both TFC and VTFC exhibited good rejection of both RB and SY dyes with all the values being greater than 98%. These high rejection values agree with the fact that the temperature for the VIP-PA was relatively high (70 °C). This made in turn a more consistent PA film with less permeance difference with the TFC membrane as compared to our previous report where the VTFC membrane was prepared at 40 °C [12]. Another fact that must be considered is the existence of a drying step (60 °C for 15 min under vacuum) after impregnating the support with MPD and before exposing the pre-membrane to TMC vapors. This drying step, which has been introduced for the first time in this manuscript, aids in removing water from the P84® support. Water molecules within the pores of the support are susceptible to reacting with TMC molecules converting carbonyl chloride groups into carboxylic groups that are significantly less reactive. Membranes without the drying step were also prepared and tested but dye rejection declines after few minutes of operation. This suggests that the presence of water molecules and humidity should be minimized prior to exposing the support containing MPD to TMC vapors in order to obtain a highly crosslinked PA layer. The performance of VTFC membranes at different reaction times (15 and 30 min) was studied. Justifying the suitability of the reaction time used for the membrane preparation, Fig. S21 shows that 15 min is insufficient to achieve a highly crosslinked PA layer and the membrane shows poor rejection. The higher permeance observed in membrane fabricated at shorter reaction time can be attributed to both the presence of defects and possibly

thinner PA selective layers.

Fig. 6 compares the membrane performance for all membranes where the PA layer has been prepared using the VIP technique. Fig. 6a shows the water permeance and RB, SY and AO rejection values along with their corresponding standard deviations and Fig. 6b displays the permeance improvement taking VTFC membranes as a reference.

Embedding ZIF-8 NPs inside the PA layer, VTFC-Z8 membrane, slightly increases the water permeance, e.g. improvements of 106%, 32%, and 21% for RB, SY and AO solutions, respectively, but compromises the rejection performance for the smallest dye AO. This suggests that the incorporation of ZIF-8 to the PA layer results in the formation of interfacial defects which creates shorter pathways for water molecules but also accounts for poor molecular sieving when using the smallest dye AO. The nature of unselective voids is often related to the agglomeration of NPs during the membrane formation process. Hydrophobic ZIF-8 may be prone to agglomeration in the aqueous MPD solution which could explain the results just mentioned. Embedding ZIF-93 NPs to prepare VTFC-Z93 membranes results in a very similar membrane performance in terms of permeance and rejection as compared to VTFC, suggesting that the dispersion of ZIF-93 within the PA matrix has a very little effect in water permeation through the membrane. This has also been observed in our previous work when comparing the NF performance of TFC and TFN membranes containing ZIF-93 [28]. ZIF-93, opposite to ZIF-8, shows hydrophilic behavior due to the presence of an aldehyde group, and therefore leads to more kinetically stable colloidal dispersions in the aqueous MPD solution preventing MOF from agglomerating and the formation of unselective voids. SEM observation revealed that both VTFC-Z93 (Fig. S9c) and VTFC (Fig. 3a) have similar membrane surface morphology: a smooth surface and absence of wrinkles and polymer veins. As previously seen in Fig. 4, the incorporation of ZIF-93 decreases the WCA of the membrane in comparison with VTFC, which seems insufficient to boost the membrane performance.

The formation of PA/ZIF bilayer VTFC membranes, B_V-Z8 and B_V-Z93, allows for an increase in water permeance while maintaining the rejection above 98% for the three dyes (Fig. 6a). The higher membrane roughness for bilayer membranes as compared to VTFC explains their higher water permeance. When comparing the performance of both bilayer membranes, the presence of hydrophilic ZIF-93 decreases the WCA, on the contrary to having a sub-layer of ZIF-8 (WCA of 75.5° and 64.4° for B_V-Z8 and B_V-Z93, respectively). Lower WCA is typically related to faster water transport which supports the higher water permeance of B_V-Z93.

We also studied the formation of ZIF-93 by WBR using a bilayer configuration, i.e. W-B_V-Z93. This membrane configuration is equivalent to B_V-Z93, which implies that the only variation between both is the procedure used to fabricate the ZIF-93 sub-layer, WBR for W-B_V-Z93 and OSR for B_V-Z93. Therefore, similar membrane performance is obtained for both membranes (Fig. 6a). Interestingly, SEM characterization showed that wrinkles and polymer veins are more prominent in W-B_V-Z93 as compared to B_V-Z93, probably due to the bigger particle sizes and more irregular shapes of the synthesized ZIF-93 NPs. This may explain the fact that water permeance in the RB and SY experiments is higher for W-B_V-Z93 as compared to B_V-Z93. Dye rejection for both B_V-Z93 and W-B_V-Z93 are all above 98% proving that the growth of a ZIF layer underneath is compatible with the formation of high-quality PA on top. In other words, crystallization of a ZIF-93 layer using an environmentally friendly process, such as the WBR, is as effective as the conventionally used crystallization method (OSR) in boosting the performance of PA membranes. In general, the bilayer strategy has obvious advantages over the conventional way of supplying MOF NPs to the skin layer of the membrane to prepare TFNs. First, it avoids the washing out of NPs during the contact of the PA monomer solutions, accumulating more suitable MOF under the PA. Second, it may avoid the excessive penetration of monomers into the support favoring the formation of more compact and continuous PA films.

Fig. 6b gives an overview of the membrane performance. For all

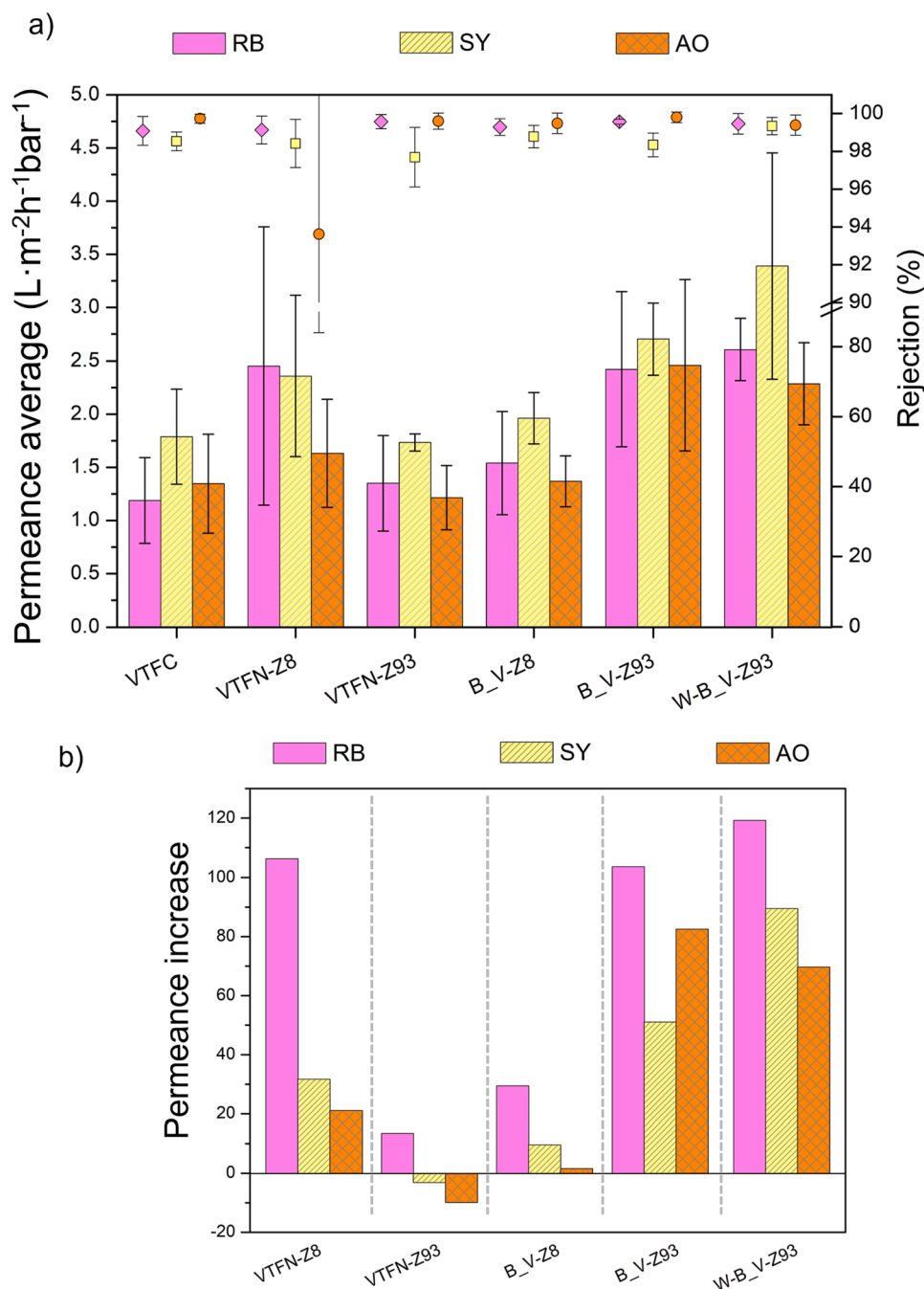


Fig. 6. Permeances and RB, SY and AO rejections of VTFC, VTFN-Z8, VTFN-Z93, B_V-Z8, B_V-Z93 and W-B_V-Z93 membranes (a) and water permeance increase as compared to VTFC (b).

membranes, the increase in water permeance follows a trend based on the size of the dye molecules, i.e. $RB > SY > AO$. The only exception is for the B_V-Z93 membrane that shows a lower increase in permeance for the SY solution than for the AO solution, which can be explained by the large standard deviation found with B_V-Z93. The highest increase in permeance is found by both PA/ZIF-93 bilayer VTFC membranes (B_V-Z93 and W-B_V-Z93) due to increased membrane hydrophilicity determined by WCA and surface roughness observed by microscopy (AFM and SEM), and thinner PA layers measured by TEM. In comparison with the control VTFC membrane, improvements in water permeance of 117%, 89% and 69% when using RB, SY and AO dye solutions, respectively, were achieved by W-B_V-Z93 membranes.

The rejection capabilities of the membranes for neutral molecules, such as PEGs, were investigated by molecular weight cut-off (MWCO)

experiments with PEG molecules of various MWs ranging from 200 to 1500 Da (Fig. S22). Both VTFC and W-B_V-Z93 membranes exhibited a MWCO between 200 and 400 Da, which is comparable to that observed for conventional PA TFC membranes commonly employed in NF applications [45–47].

The cycle stability of the prepared membranes has been assessed by undergoing them to several successive cycles for up to ca. 34 h of cumulative nanofiltration time (Fig. 7). Both VTFC and W-B_V-Z93 completed three 8 h-cycles of filtration with Rose Bengal (RB) dye, followed by two 4 h-cycles with each dye sunset yellow (SY) and acridine orange (AO). The membranes were activated with DMSO for 0.5 h before each cycle (in total four 0.5 h DMSO treatments) to remove any dye physically attached to the membrane surface and to swell polymer chains. Both VTFC and W-B_V-Z93 are capable of maintaining the initial

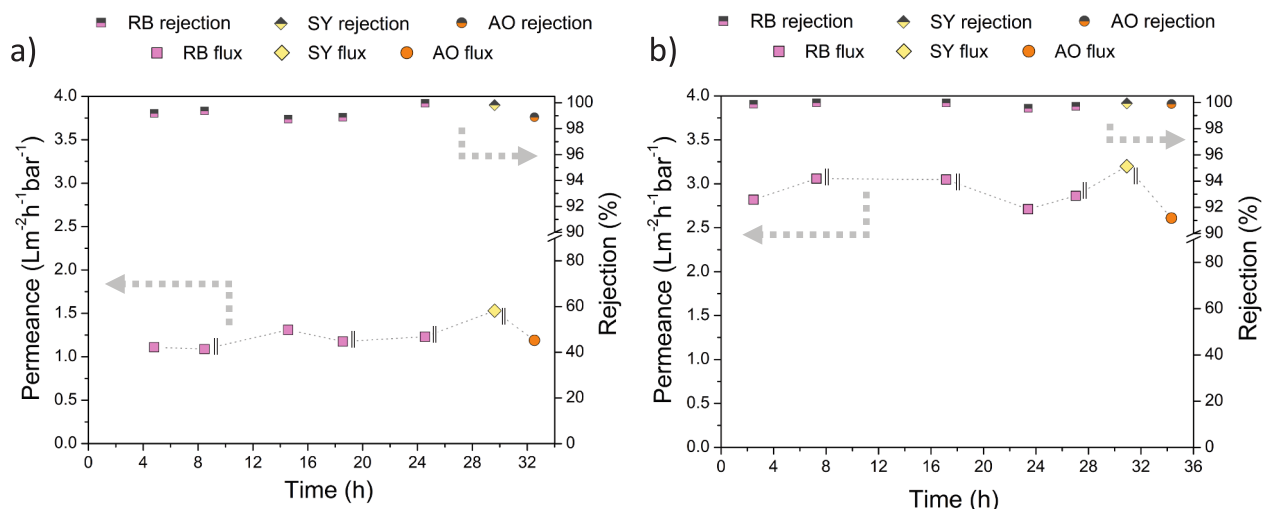


Fig. 7. Cyclic performance of VTFC (a) and W-B_Z93 membranes (b), including permeance and dye rejection for RB, SY and AO after several cycles. Double vertical bars indicate that DMSO treatment was applied to the membrane before starting each cycle, i.e. filtration with DMSO for 0.5 h at 20 bar.

flux and rejection for the entire testing period. As expected, the permeance of the W-B_Z93 membrane is higher than that of the VTFC, and SY shows the highest permeance among all three dyes for both membranes.

The performance of VTFC and W-B_Z93 was evaluated within the 3–9 pH range approximating the pH values typically seen in wastewaters. PA membranes are generally negatively charged at neutral pH due to the presence of residual carboxylic and amino groups [14,24,45]. As the pH decreases, the membrane charge shifts towards neutrality due to the protonation of these residual groups. The existence of these negatively charged functional groups on the surface is advantageous, given that the majority of organic matter and molecules dissolved in water are anionic [48]. Therefore, electrostatic repulsion between these molecules and the membrane surface enhances both permeance and rejection. Thus, for the pH filtration studies conducted in this manuscript, both anionic dyes, RB and SY, have been chosen. As the pH decreases, their anionic characteristics diminish and therefore their repulsive forces with the membrane surface. As depicted in Fig. 8, both VTFC and W-B_Z93 retain their rejection abilities throughout the entire pH range, albeit with a reduction in flux at low pH values. This decrease in flux can be attributed to the just mentioned changes in the charges of both the molecules and the

membrane surface and, consequently, dye accumulation on the membrane surface.

3.4. Economic and environmental advantages of VTFCs and Polyamide/ZIF bilayer VTFCs

The VIP method reported here for the preparation of membranes possesses several advantages over the conventional methods. Albeit heating of TMC is required, which increases the energy consumption, the absence of organic solvent has a positive influence on both the economics and the environmental impact of the manufacturing process. This method considerably reduces the amount of nasty chemicals and thus the generation of toxic waste [12]. In order to meet with disposal regulation policies, waste treatment and solvent recovery is required which is associated with high fabrication cost and detrimental environmental impact [49]. Besides, the safety of workers may be compromised when using toxic solvents or compounds such as hexane, methanol or 2-mIm. The creation of safety protocols and the use of protection equipment is mandatory by legislation which implies a significant financial cost. To sum up, the strategy proposed in this work has a strong potential to decrease the cost of the manufacturing process by

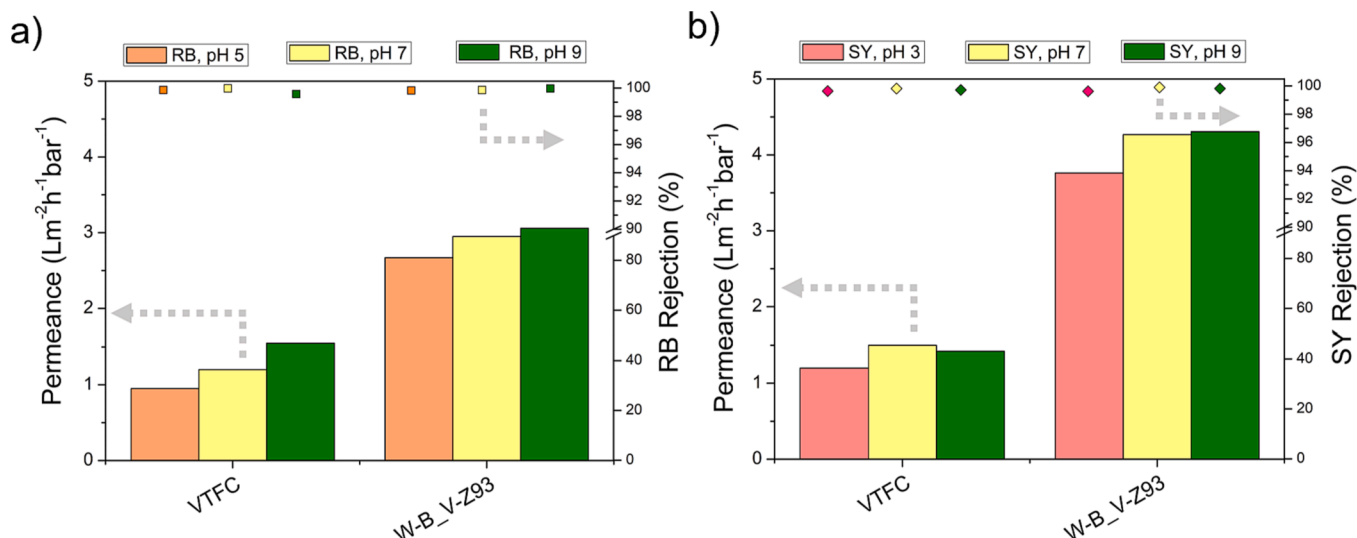


Fig. 8. Permeances and dye rejection of VTFC (a) and W-B_V-Z93 membranes (b) using RB (a) and SY (b) solutions at different pHs.

avoiding the use of toxic chemicals and, at the same time, increases the efficiency of the separation due to the enhanced membrane performance, i.e. greater volume of fresh water produced, smaller membrane areas, or lower transmembrane pressure required (less energy consumed).

Table 2 sums up all the chemicals involved in the fabrication of each type of membrane focusing on those chemicals that are toxic to humans (i.e. classified as, or suspected to be, toxic, carcinogenic, mutagenic or damaging fertility) or to the environment. From that table is evident that the two most environmentally friendly and safest procedures are VTFC followed by W-B_V-Z93. Even though the total waste generated in W-B_V-Z93 is significantly higher than in VTFC, the chemicals involved in the synthesis of ZIF-93 are relatively cheap, not harmful for humans, and the regulations for their disposal are easy to meet. On top of that, the permeance of W-B_V-Z93 is more than 2-fold higher than that of VTFC, which implies, approximately, a 117% increase in the productivity of the NF separation process or a reduction in membrane area of around 54%. As compared to B_V-Z8 and B_V-Z93 membranes, W-B_V-Z93 avoids the use of methanol and employs lower amounts of MOF chemicals ($\text{Zn}(\text{NO}_3)_2 \cdot 6\text{H}_2\text{O}$, and 2-mlm or 4-m-5-Imca) while showing a higher water permeance. VTFN-8 exhibits very similar NF performance to W-B_V-Z93, but VTFN-8 consumes a large amount of nasty chemicals. For instance, for a 500 m^2 membrane module (commercial spiral wound membrane modules are around $200\text{--}800 \text{ m}^2$) [50], 38 000 L of toxic solvent such as methanol and 800 kg of toxic 2-mlm are needed to fabricate VTFN-8 membranes due to the addition of ZIF-8, whereas W-B_V-Z93 requires from use of water and non-toxic 4-m-5-Imca instead of methanol and 2-mlm. In addition, even if the water-based route for ZIF-93 requires of a small amount of NH_4OH (0.5 mg, see Table 2), a neither non-toxic nor corrosive substance under the conditions of this study, this compensates the saving of 270 mg of methanol per cm^2 .

Another advantage of V-TFC membranes is that the synthesis is expected to be less critical to TMC monomer purity. TMC monomer is highly sensitive to humidity as chloride substitution by hydroxy groups is energetically favorable and this reaction takes place as soon as the monomer is exposed to air. Thus, monomer purification is a common practice in the preparation of PA membranes when high rejections are required. TMC having a melting point of $32\text{--}38^\circ\text{C}$ can be easily

evaporated, whereas its trisubstituted counterpart 1,3,5-benzenetricarboxylic acid exhibits a melting point above 300°C . Substitution of chloride by hydroxyl groups makes H-bond interactions between molecules possible which results in a higher melting point. Then, mild thermal conditions, as the ones employed in this work, are expected to prevent substituted monomers from evaporation whereas TMC easily reaches the membrane surface as vapor. Albeit it is not possible to assure that monosubstituted TMC does not evaporate, it is expected that most of the evaporated molecules correspond to pure TMC as monosubstitution increases the melting point and reduces the vapor pressure.

Besides, membranes prepared by the VIP procedure proposed in this manuscript has a strong potential for commercialization due to the mild synthesis conditions used, affordability of chemicals, robustness of the synthetic routes of ZIF-93 and PA, and more efficient use of the MOF (not washing off during IP since the completion of the IP is carried out without any liquid contact). When considering the scalability of PA VIP-TFC or PA/ZIF-93 bilayer VIP-TFC membranes, several aspects need to be considered. The use of organic solvent-free processes would reduce the required safety measures and minimize costs associated with residue disposal, making it highly desirable from a scalability standpoint. A main concern relates to the electricity consumption required to generate TMC vapor and the need for a humidity-free temperature-controlled reactor. However, neither of these factors is expected to pose significant challenges. Although energy is indeed necessary to heat up the TMC and facilitate vapor flow to the membrane, the temperatures used in this study are relatively moderate. For comparison, commercially available PTFE membranes are prepared at similar temperatures ($40\text{--}80^\circ\text{C}$) [51], but the synthesis of the monomer involved in PTFE polymerization requires much higher temperatures (i.e. 700°C). The membranes presented in our study require only 70°C , which is a practical temperature considering the fabrication requirements of other commercial membranes. Regarding the humidity-controlled environment, it is a known requirement in the preparation of current commercial PA TFC membranes, which also employ TMC. Controlling humidity is essential to prevent TMC monomer side reactions. Furthermore, as previously explained, our method is expected to be less sensitive to unpurified TMC as compared to conventional TFCs since TMC impurities have higher boiling points and would be minimally present in the vapor phase. This

Table 2

Comparison of chemicals used in the preparation of each type of membrane along with relevant toxicity information (source: Sigma Aldrich), amount of each chemical used per cm^2 of membrane fabricated and water permeance achieved in NF experiments with RB.

Membrane	Toxic chemicals involved	Toxic solvent involved	Excess waste generated (as compared to VTFC*) Solvents ($\text{mL}\cdot\text{cm}^{-2}$)	Reagents ($\text{mg}\cdot\text{cm}^{-2}$)	Permeance for RB solution ($\text{L}\cdot\text{m}^{-2}\cdot\text{h}^{-1}\cdot\text{bar}^{-1}$)
TFC	MPD ^{a,b,c}	n-Hexane ^{c,d,e}	n-Hexane (0.5)	TMC (1)	1.5 ± 0.3
VTFC	MPD ^{a,b,c}	–	–	–	1.2 ± 0.4
VTFN-Z8	MPD ^{a,b,c} 2-mlm ^{d,f} $\text{Zn}(\text{NO}_3)_2 \cdot 6\text{H}_2\text{O}$ ^c	Methanol ^{d,e}	Methanol (0.076)	$\text{Zn}(\text{NO}_3)_2 \cdot 6\text{H}_2\text{O}$ (0.76) 2-mlm (1.6)	2.5 ± 1.3
VTFN-Z93	MPD ^{a,b,c} $\text{Zn}(\text{NO}_3)_2 \cdot 6\text{H}_2\text{O}$ ^c	Methanol ^{d,e}	Methanol (0.025)	$\text{Zn}(\text{NO}_3)_2 \cdot 6\text{H}_2\text{O}$ (0.36) 4-m-5-Imca (1.8)	1.4 ± 0.4
B_V-Z8	MPD ^{a,b,c} 2-mlm ^{d,f} $\text{Zn}(\text{NO}_3)_2 \cdot 6\text{H}_2\text{O}$ ^c	Methanol ^{d,e}	Methanol (0.34)	$\text{Zn}(\text{NO}_3)_2 \cdot 6\text{H}_2\text{O}$ (23)	1.5 ± 0.5
B_V-Z93	MPD ^{a,b,c} $\text{Zn}(\text{NO}_3)_2 \cdot 6\text{H}_2\text{O}$ ^c	Methanol ^{d,e}	1-Octanol (0.16) Methanol (0.34)	2-mlm (10) $\text{Zn}(\text{NO}_3)_2 \cdot 6\text{H}_2\text{O}$ (23)	2.4 ± 0.7
W-B_V-Z93	MPD ^{a,b,c} $\text{Zn}(\text{NO}_3)_2 \cdot 6\text{H}_2\text{O}$ ^c	–	1-Octanol (0.16) H_2O (1)	4-m-5-Imca (14) $\text{Zn}(\text{NO}_3)_2 \cdot 6\text{H}_2\text{O}$ (10) 4-m-5-Imca (7.7) $(\text{NH}_4)\text{OH}$ (0.5) ^c	2.6 ± 0.3

^a Toxic to humans.

^b Suspected of causing genetic defects.

^c Toxic to aquatic life.

^d Suspected of damaging fertility.

^e May cause damage to organs.

^f Suspected of causing cancer.

* Chemicals involved in the preparation of VTFC include MPD ($10 \text{ mg}\cdot\text{cm}^{-2}$), H_2O ($0.5 \text{ mL}\cdot\text{cm}^{-2}$) and TMC ($2.5\cdot 10^{-4} \text{ mg}\cdot\text{cm}^{-2}$). These chemicals are common to all membranes. Then, the column “Excess waste generated” refers to chemicals used in the membrane fabrication process excluding those chemicals common to all membranes. The amount of TMC evaporated has been calculated according to that reported by Paseta et al. [12].

suggests that our approach is less affected by TMC purity concerns.















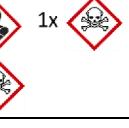

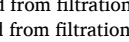
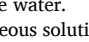
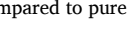
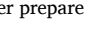



3.5. Comparison with literature

With the purpose of establishing a reliable comparison between the membranes investigated in our study and those previously reported by other authors, Table 3 sums up several studies involving TFCs of PA together with ZIF-8 and ZIF-93 NPs. The membranes presented in our work offer some attractive advantages over these studies. As discussed in the introduction, the incorporation of ZIF-8 to PA, either as a TFN or as a

bilayer, often leads to an improvement in water permeance. Wang et al. [25] reported a 182% increase in water permeance as a result of the formation of bilayer ZIF-8/PA TFCs membranes, which is the highest improvement value amongst all PA/ZIF-8 membranes in Table 3. However, this value was obtained from filtration with pure water and may differ from that obtained when using dye or salt solutions due to pore blockage and concentration polarization effects. For instance, in a similar bilayer PA/ZIF-8 strategy, Zhao et al. [23] reported a 30% increase in water permeance for filtrations of aqueous solutions of NaCl and xylose. Methods involving ZIF-93 and PA draw similar conclusions.

Table 3

Summary of similar works reported in the literature and comparison of their toxicity using the Health Hazards and Toxic pictograms, the improvement in water permeance as compared to the control pure PA membrane, and dye/salt rejection of the smallest molecule tested.

Membrane configuration used	Health Hazards and Toxic pictograms	Water permeance as increase compared to pure PA layer (%)	Dye/salt rejection of the smallest molecule tested	Ref.
TFN_PA/ZIF-8	3x  2x 	27% ^a	61% xylose (150 Da)	[23]
Bilayer TFC_PA/ZIF-8	3x  2x 	30% ^a	62% xylose (150 Da)	[23]
TFN_PA/ZIF-8	3x  2x 	133% ^b	<90% Methylene Blue (320 Da)	[24]
Bilayer TFC_PA/ZIF-8	3x  2x 	91% ^b	<90% Methylene Blue (320 Da)	[24]
Bilayer TFC_PA/ZIF-8	3x  2x 	182% ^b	>99% Congo Red (697 Da)	[25]
TFN_PA/ZIF-93	2x  2x 	0% ^c	>99% naproxen (230 Da)	[28]
Bilayer TFC_PA/ZIF-93	2x  2x 	144–256% ^c	>99% naproxen (230 Da)	[28]
Bilayer TFC_PA/ZIF-93/ SWCNT	2x  2x 	90–112% ^d	>96% AO (265 Da)	[29]
Bilayer VTFC_PA/ZIF-93	1x  1x 	69–117% ^{d,e}	>99% AO (265 Da)	This work
VTFC_PA	1x  1x 	–	<95% AO (265 Da)	[12]
VTFC_Polyester CD-TMC	1x  1x 	200–300% ^e	62% Methyl Orange (327 Da)	[13]
VTFC_PA/COOH-TiO ₂	1x 	85% ^e	87% Na ₂ SO ₄	[14]

^a Membrane permeance calculated from filtration of NaCl and xylose.

^b Membrane permeance calculated from filtration of pure water.

^c Membrane permeance calculated from filtration of aqueous solutions of pharmaceutical compounds.

^d Membrane permeance calculated from filtration of aqueous solutions of RB, SY and AO dyes.

^e Water permeance as increase compared to pure PA layer prepare by VIP.

Paseta et al. studied both TFN and bilayer PA/ZIF-93 membranes for filtrations of pharmaceutical compounds and found the latest configuration more successful. The authors reported a maximum increase in water permeance ranging from 144 to 256% depending upon the filtration solution, which suggests a significant influence of the rejecting molecules on the water permeance [28]. Berned-Samatan et al. [29] showed an improvement of water permeance ranging from 90 to 112% when using bilayer TFCs of PA/ZIF-93 over SWCNT supports for water NF of RB, SY and AO solutions. Results shown in our study report a 69–117% increase in water permeance for filtration of the same dye solutions that were used by Berned-Samatan et al., which suggests that membranes presented in our work are of the same quality as those previously reported but allows for a drastic reduction of the amount of toxic reagent/solvent used.

Table 3 also includes all existing studies focused on the formation of PA TFCs via a VIP technique. This approach was firstly reported by our research group [12]. Although the prepared membranes achieved acceptable rejection for RB dyes, the rejection was compromised for the smaller ones, SY and AO. However, our current work demonstrates, as discussed in the previous section, that the VIP membranes can show enhanced water permeances with high rejections to low MW dyes such as AO. These experimental findings can be attributed to many factors, including: i) higher temperature used in this study, and ii) incorporation of a drying step to reduce humidity that has been shown to react with TMC giving rise to poorly cross-linked PA layers. Li et al. [13] prepared VTFCs membranes based on polycondensation reactions between piperazine or β -cyclodextrins and TMC which achieved modest rejections with values above 90% only for organic dyes larger than 400 Da. These membranes showed high water flux and reduced the amount of toxic waste as compared to conventional TFCs due to the use of a VIP technique for polymerization, but their rejection performance was notably poorer than these presented in our current study, using an optimized VIP process, capable of rejecting 99% of AO dye (MW of 265 Da). In another work, Karki et al. [14] reported the fabrication of PA membranes by VIP made of diethylenetriamine and TMC and containing TiO₂ nanoparticles (NPs) for heavy metal ions removal. The use of diethylenetriamine instead of MPD resulted in a “less toxic” membrane fabrication process but severely impacted on the membrane performance. In fact, MPD is commonly considered the preferred option for the preparation of PA TFC membranes, as it offers the best trade-off between water permeance and solute rejection.

Apart from the membranes presented in Table 3, other filler/polymer combinations have recently shown promising results. For example, Zhang et al. [52] reported on a ZIF-8/poly(sodium 4-styrenesulfonate) membrane that was prepared by a coordination-driven in situ self-assembly method, which produced a selective hybrid layer with a thickness of approximately 1.5 μ m. The resulting membrane exhibited a permeance of 26.5 LMH bar⁻¹ and a rejection of 98.6% for methyl blue (800 Da), demonstrating that the incorporation of ZIF-8 can help overcome the typical trade-off between permeability and selectivity. Denny et al. [17] developed a straightforward method to create uniform MOF-polymer composite MMMs with significant MOF content (~67 wt%). This method is applicable to a diverse range of MOFs (including ZIF-8) and can easily produce robust, large-scale, and flexible free-standing MMMs with excellent mechanical properties. Besides, the MOFs present in these MMMs maintain a high level of crystallinity, porosity, and accessibility, making them suitable for postsynthetic chemical modifications. The prepared UiO-66/PVDF MMMs were capable of removing 95% and 20% of Coomassie brilliant blue R-250 (826 Da) and methyl orange (327 Da) dyes, respectively.

In line with the idea explained in this paper of aiming to create membranes through more sustainable methods, few attempts have been made to remove MPD molecules. For example, mussel-inspired sulfonated dopamine was used as a monomer along with TMC to produce TFCs over PAN support. The resulting membranes exhibit a competitive flux of 10 LHM bar⁻¹ and acceptable rejection of 99% for all dyes,

methylene blue (320 Da), Brilliant green (403 Da), Congo red (696 Da), and Methyl blue (799 Da) [53].

PES membranes are commonly employed for ultrafiltration applications. However, they are not suitable for nanofiltration due to their inadequate rejection performance for low MW compounds. Functionalization of graphene oxide nanofillers and incorporation into PES matrix together with pore forming agents was proposed as a strategy to modify the flux and rejection properties of these membranes [54]. The best performing membranes achieved a pure water flux of 9.9 LMHbar⁻¹ and 99% rejection of SY and AO dyes. This performance establishes PES membranes as a promising alternative to PA membranes, but their high susceptibility to swelling when interacting with organic molecules limits their applicability to complex water streams. Crosslinked PVDF membranes have been reported for application at extreme pH conditions [55]. These membranes exhibited a water permeance of 0.7 LMHbar⁻¹ and demonstrated adequate dye rejection (100% for RB and 91% for methyl orange) under both highly alkaline conditions (5 M NaOH) and highly acidic conditions (5 M HCl).

4. Conclusions

We have established more efficient conditions (higher temperature and shorter PA interfacial polymerization time) for the preparation of thin film composite nanofiltration membranes with a VIP method that excludes the use of organic solvents. In addition, with this method both ZIF-8 and ZIF-93 can be incorporated into TFN membranes and bilayer PA/ZIF membranes. The highest enhancement in permeance without compromising dye rejections was achieved with PA/ZIF-93 bilayer VTFC membrane. Moreover, a synthetic route that only involves water as a solvent, so-called WBR, was developed for the growth of ZIF-93, which, in combination with the VIP procedure for the synthesis of PA, allows for the fabrication of PA/ZIF-93 bilayer membranes without the use of organic solvents. PA/ZIF-93 (by WBR) bilayer VTFC membranes achieved 117%, 89% and 69% of permeance improvement as compared to bare (with no MOFs) VTFC membranes when using RB, SY and AO dyes, respectively, maintaining all dye rejections above 99%. Membrane characterization suggests that the increase in membrane permeance is due to the following effects produced by the introduction of a sub-layer of ZIF-93: i) higher membrane surface due to the increase of roughness, which has been analyzed by SEM and AFM, ii) enhanced membrane hydrophilicity, as revealed by WCA measurements, due to more MOF (hydrophilic ZIF-93) located under the PA layer, and iii) thinner PA layers according to TEM imaging. The prepared VTFC and bilayer VTFC membranes were evaluated for cycle stability for up to ca. 34 h of cumulative nanofiltration time. Both VTFC and PA/ZIF-93 (by WBR) bilayer VTFC membranes maintained their initial flux and rejection throughout the investigation period. In addition, bilayer VTFC membranes were also subjected to filtration with RB and SY solutions at varying pHs ranging from 3 to 9, demonstrating no discernible changes in their rejection properties.

Funding

This work was supported by Grant PID2019-104009RB-I00 funded by MCIN/AEI/10.13039/501100011033 («Agencia Estatal de Investigación» (AEI) and «Ministerio de Ciencia e Innovación» (MCIN), Spain); Margarita Salas and Juan de la Cierva programmes funded by Spanish Ministerio de Universidades and the European Union-NextGenerationEU Fund; Grant RYC2019-027060-I funded by MICIN/AEI/10.13039/501100011033 and by “ESF Investing in your future”; and financial support from the Aragón Government (Grant T68-23R).

Declaration of Competing Interest

The authors declare that they have no known competing financial interests or personal relationships that could have appeared to influence

the work reported in this paper.

Data availability

No data was used for the research described in the article.

Acknowledgment

Grant PID2019-104009RB-I00 funded by MCIN/AEI/10.13039/501100011033 («Agencia Estatal de Investigación» (AEI) and «Ministerio de Ciencia e Innovación» (MCIN), Spain). J. M. Luque-Alled acknowledges the Spanish Ministerio de Universidades and the European Union-NextGenerationEU Fund for funding through the Margarita Salas and Juan de la Cierva programmes. Patricia Gorgojo is supported by Grant RYC2019-027060-I funded by MICIN/AEI/10.13039/501100011033 and by «ESF Investing in your future». Financial support from the Aragón Government (T68-23R) is gratefully acknowledged. Authors would like to acknowledge the use of Servicio General de Apoyo a la Investigación-SAI and the use of instrumentation as well as the technical advice provided by the National Facility ELECMI ICTS, node «Laboratorio de Microscopías Avanzadas (LMA)», both at «Universidad de Zaragoza».

Appendix A. Supplementary data

Supplementary data to this article can be found online at <https://doi.org/10.1016/j.cej.2023.144233>.

References

- M.M. Pendergast, E.M.V. Hoek, A review of water treatment membrane nanotechnologies, *Energ. Environ. Sci.* 4 (6) (2011) 1946–1971, <https://doi.org/10.1039/c0ee00541j>.
- A. De Munari, A.J.C. Semiao, B. Antizar-Ladislao, Retention of pesticide Endosulfan by nanofiltration: influence of organic matter-pesticide complexation and solute-membrane interactions, *Water Res.* 47 (10) (2013) 3484–3496, <https://doi.org/10.1016/j.watres.2013.03.055>.
- I. Vergili, Application of nanofiltration for the removal of carbamazepine, diclofenac and ibuprofen from drinking water sources, *J. Environ. Manage.* 127 (2013) 177–187, <https://doi.org/10.1016/j.jenvman.2013.04.036>.
- S. Sanches, A. Penetra, A. Rodrigues, E. Ferreira, V.V. Cardoso, M.J. Benoliel, M.T. B. Crespo, V.J. Pereira, J.G. Crespo, Nanofiltration of hormones and pesticides in different real drinking water sources, *Sep. Purif. Technol.* 94 (2012) 44–53, <https://doi.org/10.1016/j.seppur.2012.04.003>.
- R.S. Harisha, K.M. Hosamani, R.S. Keri, S.K. Nataraj, T.M. Aminabhavi, Arsenic removal from drinking water using thin film composite nanofiltration membrane, *Desalination* 252 (1–3) (2010) 75–80, <https://doi.org/10.1016/j.desal.2009.10.022>.
- A. Figoli, A. Cassano, A. Criscuoli, M.S.I. Mozumder, M.T. Uddin, M.A. Islam, E. Drioli, Influence of operating parameters on the arsenic removal by nanofiltration, *Water Res.* 44 (1) (2010) 97–104, <https://doi.org/10.1016/j.watres.2009.09.007>.
- R. Atrai, G. Vatai, E. Bekassy-Molnar, A. Balint, Investigation of ultra- and nanofiltration for utilization of whey protein and lactose, *J. Food Eng.* 67 (3) (2005) 325–332, <https://doi.org/10.1016/j.jfoodeng.2004.04.035>.
- J.F. Kim, G. Szekely, I.B. Valtcheva, A.G. Livingston, Increasing the sustainability of membrane processes through cascade approach and solvent recovery-pharmaceutical purification case study, *Green Chem.* 16 (1) (2014) 133–145, <https://doi.org/10.1039/c3gc41402g>.
- M.a. Markets, Membrane Separation Systems Market - Global Industry Analysis, Size, Share, Growth, Trends, and Forecast 2017 - 2025, 2017.
- M. Qasim, M. Badrelzaman, N.N. Darwish, N.A. Darwish, N. Hilal, Reverse osmosis desalination: a state-of-the-art review, *Desalination* 459 (2019) 59–104, <https://doi.org/10.1016/j.desal.2019.02.008>.
- Z. Ali, Y. Wang, W. Ogieglo, F. Pacheco, H. Vovusha, Y.u. Han, I. Pinnau, Gas separation and water desalination performance of defect-free interfacially polymerized para-linked polyamide thin-film composite membranes, *J. Membr. Sci.* 618 (2021) 118572.
- L. Paseta, C. Echaide-Gorri, C. Tellez, J. Coronas, Vapor phase interfacial polymerization: a method to synthesize thin film composite membranes without using organic solvents, *Green Chem.* 23 (6) (2021) 2449–2456, <https://doi.org/10.1039/d1gc00236h>.
- W.B. Li, Z. Yang, W.L. Yang, H. Guo, C.Y. Tang, Vapor-phase polymerization of high-performance thin-film composite membranes for nanofiltration, *AIChE J* 68 (2) (2022), <https://doi.org/10.1002/aic.17517>.
- S. Karki, P.G. Ingole, Development of polymer-based new high performance thin-film nanocomposite nanofiltration membranes by vapor phase interfacial polymerization for the removal of heavy metal ions, *J. Chem. Eng.* 446 (2022) 137303.
- G. Obey, M. Adelaide, R. Ramaraj, Biochar derived from non-customized matamba fruit shell as an adsorbent for wastewater treatment, *Journal of Bioresources and Bioproducts* 7 (2) (2022) 109–115.
- J. Jagwe, P.W. Olupot, E. Meny, H.M. Kalibbala, Synthesis and application of granular activated carbon from biomass waste materials for water treatment: a review, *Journal of Bioresources and Bioproducts* 6 (4) (2021) 292–322.
- M.S. Denny, S.M. Cohen, In situ modification of metal-organic frameworks in mixed-matrix membranes, *Angewandte Chemie-International Edition* 54 (31) (2015) 9029–9032, <https://doi.org/10.1002/anie.201504077>.
- R. Banerjee, A. Phan, B. Wang, C. Knobler, H. Furukawa, M. O’Keeffe, O.M. Yaghi, High-throughput synthesis of zeolitic imidazolate frameworks and application to CO₂ capture, *Science* 319 (5865) (2008) 939–943, <https://doi.org/10.1126/science.1152516>.
- Y.C. Pan, Y.Y. Liu, G.F. Zeng, L. Zhao, Z.P. Lai, Rapid synthesis of zeolitic imidazolate framework-8 (ZIF-8) nanocrystals in an aqueous system, *Chem. Comm.* 47 (7) (2011) 2071–2073, <https://doi.org/10.1039/c0cc05002d>.
- J. Cravillon, S. Munzer, S.J. Lohmeier, A. Feldhoff, K. Huber, M. Wiebecke, Rapid room-temperature synthesis and characterization of nanocrystals of a prototypical zeolitic imidazolate framework, *Chem. Mater.* 21 (8) (2009) 1410–1412, <https://doi.org/10.1021/cm900166h>.
- Y.R. Lee, M.S. Jang, B.Y. Cho, H.J. Kwon, S. Kim, W.S. Ahn, ZIF-8: a comparison of synthesis methods, *J. Chem. Eng.* 271 (2015) 276–280, <https://doi.org/10.1016/j.cej.2015.02.094>.
- K.S. Park, Z. Ni, A.P. Cote, J.Y. Choi, R.D. Huang, F.J. Uribe-Romo, H.K. Chae, M. O’Keeffe, O.M. Yaghi, Exceptional chemical and thermal stability of zeolitic imidazolate frameworks, *PNAS* 103 (27) (2006) 10186–10191, <https://doi.org/10.1073/pnas.0602439103>.
- Y.Y. Zhao, Y.L. Liu, X.M. Wang, X. Huang, Y.F.F. Xie, Impacts of metal-organic frameworks on structure and performance of polyamide thin-film nanocomposite membranes, *ACS Appl. Mater. Interfaces* 11 (14) (2019) 13724–13734, <https://doi.org/10.1021/acsami.9b01923>.
- X. Wu, L. Yang, F. Meng, W. Shao, X. Liu, M. Li, ZIF-8-incorporated thin-film nanocomposite (TFN) nanofiltration membranes: importance of particle deposition methods on structure and performance, *J. Membr. Sci.* 632 (2021) 119356.
- L.Y. Wang, M.Q. Fang, J. Liu, J. He, J.D. Li, J.D. Lei, Layer-by-layer fabrication of high-performance polyamide/ZIF-8 nanocomposite membrane for nanofiltration applications, *ACS Appl. Mater. Interfaces* 7 (43) (2015) 24082–24093, <https://doi.org/10.1021/acsami.5b07128>.
- M.D. Li, J.J. Liu, S.P. Deng, Q. Liu, N. Qi, Z.Q. Chen, Low-pressure CO₂ capture in zeolite imidazolate frameworks with ultramicropores studied by positron annihilation, *ACS Appl. Energy Mater.* 4 (8) (2021) 7983–7991, <https://doi.org/10.1021/acsami.1c01297>.
- D. Madhav, M. Malankowska, J. Coronas, Synthesis of nanoparticles of zeolitic imidazolate framework ZIF-94 using inorganic deprotonators, *New J. Chem.* 44 (46) (2020) 20449–20457, <https://doi.org/10.1039/d0nj04402d>.
- L. Paseta, D. Antoran, J. Coronas, C. Tellez, 110th Anniversary: polyamide/metal-organic framework bilayered thin film composite membranes for the removal of pharmaceutical compounds from water, *Ind. Eng. Chem. Res.* 58 (10) (2019) 4222–4230, <https://doi.org/10.1021/acs.iecr.8b06017>.
- V. Berned-Samatán, C. Rubio, A. Galán-González, E. Muñoz, A.M. Benito, W. K. Maser, J. Coronas, C. Tellez, Single-walled carbon nanotube buckypaper as support for highly permeable double layer polyamide/zeolitic imidazolate framework in nanofiltration processes, *J. Membr. Sci.* 652 (2022) 120490.
- L. Martinez-Izquierdo, C. Tellez, J. Coronas, Highly stable Pebax (R) Renew (R) thin-film nanocomposite membranes with metal organic framework ZIF-94 and ionic liquid Bmim BF₄ for CO₂ capture, *J. Mater. Chem. A* 10 (36) (2022) 18822–18833, <https://doi.org/10.1039/d2ta03958c>.
- L. Paseta, M. Navarro, J. Coronas, C. Tellez, Greener processes in the preparation of thin film nanocomposite membranes with diverse metal-organic frameworks for organic solvent nanofiltration, *J. Ind. Eng. Chem.* 77 (2019) 344–354, <https://doi.org/10.1016/j.jiec.2019.04.057>.
- E.V. Ramos-Fernandez, A. Grau-Artienza, D. Farrusseng, S. Aguado, A water-based room temperature synthesis of ZIF-93 for CO₂ adsorption, *J. Mater. Chem. A* 6 (14) (2018) 5598–5602, <https://doi.org/10.1039/c7ta09807c>.
- M.F.J. Solomon, Y. Bhole, A.G. Livingston, High flux membranes for organic solvent nanofiltration (OSN)-interfacial polymerization with solvent activation, *J. Membr. Sci.* 423 (2012) 371–382, <https://doi.org/10.1016/j.memsci.2012.08.030>.
- T.C.C.D.C. (CCDC), <https://www.ccdc.cam.ac.uk/>.
- R.C.S.R. (RCSR), <http://rcsr.anu.edu.au/>.
- F. Cacho-Bailo, C. Tellez, J. Coronas, Interactive thermal effects on metal-organic framework polymer composite membranes, *Chemistry-A European Journal* 22 (28) (2016) 9533–9536, <https://doi.org/10.1002/chem.201601530>.
- F. Akbari Beni, M. Niknam Shahrak, Alkali metals-promoted capacity of ZIF-8 and ZIF-90 for carbon capturing: a molecular simulation study, *Polyhedron* 178 (2020) 114338.
- Y. Li, L.H. Wee, J.A. Martens, I.F.J. Vankelecom, Interfacial synthesis of ZIF-8 membranes with improved nanofiltration performance, *J. Membr. Sci.* 523 (2017) 561–566, <https://doi.org/10.1016/j.memsci.2016.09.065>.
- K.G. Ray, D.L. Olmsted, J.M.R. Burton, Y. Houndonougbo, B.B. Laird, M. Asta, Gas membrane selectivity enabled by zeolitic imidazolate framework electrostatics, *Chem. Mater.* 26 (13) (2014) 3976–3985, <https://doi.org/10.1021/cm5015477>.
- M.E. Casco, Y.Q. Cheng, L.L. Daemen, D. Fairen-Jimenez, E.V. Ramos-Fernandez, A.J. Ramirez-Cuesta, J. Silvestre-Albero, Gate-opening effect in ZIF-8: the first

- experimental proof using inelastic neutron scattering, *Chem. Comm.* 52 (18) (2016) 3639–3642, <https://doi.org/10.1039/c5cc10222g>.
- [41] C. Van Goethem, R. Verbeke, S. Hermans, R. Bernstein, I.F.J. Vankelecom, Controlled positioning of MOFs in interfacially polymerized thin-film nanocomposites, *J. Mater. Chem. A* 4 (42) (2016) 16368–16376, <https://doi.org/10.1039/c6ta05175h>.
- [42] S. Sorribas, P. Gorgojo, C. Tellez, J. Coronas, A.G. Livingston, High flux thin film nanocomposite membranes based on metal-organic frameworks for organic solvent nanofiltration, *J. Am. Chem. Soc.* 135 (40) (2013) 15201–15208, <https://doi.org/10.1021/ja407665w>.
- [43] C. Van Goethem, R. Verbeke, M. Pfanmoller, T. Koschine, M. Dickmann, T. Timpel-Lindner, W. Egger, S. Bals, I.F.J. Vankelecom, The role of MOFs in thin-film nanocomposite (TFN) membranes, *J. Membr. Sci.* 563 (2018) 938–948, <https://doi.org/10.1016/j.memsci.2018.06.040>.
- [44] C.Y.Y. Tang, Y.N. Kwon, J.O. Leckie, Effect of membrane chemistry and coating layer on physiochemical properties of thin film composite polyamide RO and NF membranes I FTIR and XPS characterization of polyamide and coating layer chemistry, *Desalination* 242 (1–3) (2009) 149–167, <https://doi.org/10.1016/j.desal.2008.04.003>.
- [45] C.M. Zhou, Y.L. Shi, C.S. Sun, S.C. Yu, M.H. Liu, C.J. Gao, Thin-film composite membranes formed by interfacial polymerization with natural material sericin and trimesoyl chloride for nanofiltration, *J. Membr. Sci.* 471 (2014) 381–391, <https://doi.org/10.1016/j.memsci.2014.08.033>.
- [46] V.T. Do, C.Y. Tang, M. Reinhard, J.O. Leckie, Effects of hypochlorous acid exposure on the rejection of salt, polyethylene glycols, boron and arsenic(V) by nanofiltration and reverse osmosis membranes, *Water Res.* 46 (16) (2012) 5217–5223, <https://doi.org/10.1016/j.watres.2012.06.044>.
- [47] M. Dalwani, N.E. Benes, G. Bargeman, D. Stamatialis, M. Wessling, Effect of pH on the performance of polyamide/polyacrylonitrile based thin film composite membranes, *J. Membr. Sci.* 372 (1–2) (2011) 228–238, <https://doi.org/10.1016/j.memsci.2011.02.012>.
- [48] D. Rana, T. Matsuura, Surface Modifications for Antifouling Membranes, *Chem. Rev.* 110 (4) (2010) 2448–2471, <https://doi.org/10.1021/cr800208y>.
- [49] P. Marchetti, M.F.J. Solomon, G. Szekely, A.G. Livingston, Molecular separation with organic solvent nanofiltration: a critical review, *Chem. Rev.* 114 (21) (2014) 10735–10806, <https://doi.org/10.1021/cr500006j>.
- [50] J.D. Seader, E.J. Henley, *Separation Process Principles*, Separation Process Principles 2005.
- [51] G.J. Puts, P. Crouse, B.M. Ameduri, Polytetrafluoroethylene: synthesis and characterization of the original extreme polymer, *Chem. Rev.* 119 (3) (2019) 1763–1805, <https://doi.org/10.1021/acs.chemrev.8b00458>.
- [52] R. Zhang, S.L. Ji, N.X. Wang, L. Wang, G.J. Zhang, J.R. Li, Coordination-driven in situ self-assembly strategy for the preparation of metal-organic framework hybrid membranes, *Angewandte Chemie-International Edition* 53 (37) (2014) 9775–9779, <https://doi.org/10.1002/anie.201403978>.
- [53] J. Ding, H. Wu, P. Wu, Development of nanofiltration membranes using mussel-inspired sulfonated dopamine for interfacial polymerization, *J. Membr. Sci.* 598 (2020) 117658.
- [54] J.M. Luque-Alled, A. Abdel-Karim, M. Alberto, S. Leaper, M. Perez-Page, K. Huang, A. Vijayaraghavan, A.S. El-Kalliny, S.M. Holmes, P. Gorgojo, Polyethersulfone membranes: From ultrafiltration to nanofiltration via the incorporation of APTS functionalized-graphene oxide, *Sep. Purif. Technol.* 230 (2020) 115836.
- [55] C. Van Goethem, M. Mertens, I.F.J. Vankelecom, Crosslinked PVDF membranes for aqueous and extreme pH nanofiltration, *J. Membr. Sci.* 572 (2019) 489–495, <https://doi.org/10.1016/j.memsci.2018.11.036>.